

## OPEN CLUSTERS AND ASSOCIATIONS IN THE GAIA ERA

Estelle Moraux<sup>1,2</sup>

**Abstract.** Open clusters and associations are groups of young stars, respectively bound and unbound, that share the same origin and disperse over time into the galactic field. As such, their formation and evolution are the key to understand the origin and properties of galactic stellar populations. Moreover, since their members have about the same age, they are ideal laboratories to study the properties of young stars and constrain stellar evolution theories.

In this contribution, I present our current knowledge on open clusters and associations. I focus on the methods used to derive the statistical properties (IMF, spatial distribution, IMF) of young stars and briefly discuss how they depend on the environment. I then describe how open clusters can be used as probes to investigate the structure, dynamics and chemical composition of the Milky Way. I conclude by presenting the Gaia mission and discuss how it will revolutionize this field of research.

### 1 Introduction

It is commonly said that stars form in “clusters”. However it would be more correct to say that stars form in groups with  $N = 10$  to  $10^5$  and a distinction should be made between young open clusters and associations. While both of them correspond to physically associated groups of population I stars, sharing the same origin and moving together through the Galaxy, a cluster is gravitationally bound and an association is not.

Observationally, a cluster (like the Pleiades) shows a clear concentration of young stars above the surrounding stellar background while an association corresponds to a region where there is a higher than normal density of O-B stars (OB associations, such as Orion OB1) or T-Tauri stars (T associations, like TW Hydra). The average stellar density of open clusters can go from 0.1 to about 10

---

<sup>1</sup> Univ. Grenoble Alpes, IPAG, F-38000 Grenoble, France

<sup>2</sup> CNRS, IPAG, F-38000 Grenoble, France

e-mail: [estelle.moraux@univ-grenoble-alpes.fr](mailto:estelle.moraux@univ-grenoble-alpes.fr)

stars/pc<sup>3</sup> in a typical diameter of a few parsecs, yielding a few tens to 10<sup>5</sup> stars. An association contains typically 10 to 1000 stars which are spread over a much wider area (several tens to a few hundred parsecs in diameter), corresponding to a stellar density of  $\sim 0.01$  stars/pc<sup>3</sup> or less (see Figure 1).

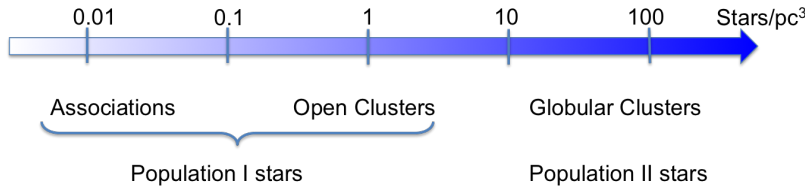


**Fig. 1.** Typical density of associations, open clusters and globular clusters.

Another difference between a cluster and an association arising directly from their definition is the lifetime. An open cluster is loosely bound and its star members will stay together for about 100 Myr to a few Gyr for the densest ones, before it gets disrupted by the galactic tidal field. On the contrary, an association is unbound and disperses rapidly, over a timescale of 10 to 100 Myr.

This means that it is much more difficult to detect associations and get a full census of their population. Very large areas of the sky need to be covered to identify a few members among thousands of unrelated field stars based on colors or proper motions. In particular, Hipparcos data have been very powerful in detecting OB association (e.g. De Zeeuw et al. 1999). However, caution must be taken when using kinematic informations for  $\sim 100$  Myr associations as lots of field objects may share the same proper motion due to resonant trap in the galactic field (e.g. ABDor; Famaey et al. 2008). To date, about 80 O-B associations and 3000 open clusters are known in the solar neighborhood (up to  $\sim 1.8$  kpc; Kharchenko et al. 2013), but they may be up to 10<sup>5</sup> in the Galaxy.

Despite the above differences, open clusters and associations show strong similarities. They are located in the arms of the Milky Way and other spiral galaxies, they are composed of young stars that recently formed in the disks of galaxies, and they continue to form (as opposed to globular clusters). All the stars belonging to the same cluster/association have the same age (with maybe a spread of a few Myr) and metallicity, having formed from the same cloud of gas and dust. Open clusters and associations can therefore be used to probe the galactic disk structure and formation rate, as well as to study the young star properties and their formation process. Where does the galactic disk population come from: open cluster, association, or both? Is there any preferred mode of star formation? Do clusters and associations form similarly but evolve differently or do they form from different physical conditions (density, turbulence, magnetic field...)? How does the cluster/association environment affect the stellar properties?

In order to be able to answer the above questions, we first need to be able to distinguish a cluster from an association, or in other words to know whether a stellar group is gravitationally bound or not. The total energy of a system is

$E = T + U$  with  $U = -GM_c^2/R_g$  the potential energy, and  $T = \frac{1}{2}M_c\sigma_v^2$  the kinetic energy.  $M_c$  is the cluster mass,  $R_g$  the *gravitational* radius and  $\sigma_v$  the 3D velocity dispersion. A system is bound if  $E < 0$ , i.e., if  $\sigma_v < \sqrt{2\frac{GM_c}{R_g}}$  or  $\sigma_v < \sqrt{2}\sigma_v^{vir}$  where  $\sigma_v^{vir}$  corresponds to the *virialized* velocity dispersion given by  $2T + U = 0$ . Therefore a subvirial or virialized system is bound while a supervirial system can be marginally bound or unbound.

In practice, it is not such an easy task to know the dynamical state of a stellar group as one first needs to estimate its mass, gravitational radius, and 3D velocity dispersion. Masses are estimated either directly by summing up individual masses, or indirectly from the tidal radius. Indeed  $M_c = \frac{4A(A-B)r_t^3}{G}$  (King 1962) where A and B are the Oort constants and  $r_t$  is the tidal radius.  $R_g$  is usually derived from the core radius  $r_c$  ( $\sim 0.2 - 0.3R_g$ ) that is obtained by fitting a King distribution to the radial profile – but this can only be done if the group is centrally concentrated. Typical values for open cluster core radii are 1-2 pc and 10-25 pc for tidal radii. The velocity dispersions in open clusters are typically only a few km/s, indicating that individual stellar velocities have to be measured with an accuracy  $< 1$ km/s which requires high resolution spectroscopic observations. Moreover  $\sigma_v$  has to be corrected from bias introduced by binaries (e.g. Cottaar & Hénault-Brunet 2014, Cottaar et al. 2012). Recent studies have shown that among the young massive star clusters Westerlund 1 is subvirial and strongly bound (Cottaar et al. 2012) while NGC3603 is about virialized and marginally bound (Pang et al. 2013). The Cyg OB2 association is indeed unbound (Kiminki et al. 2007, 2008; Wright et al. 2014) but does not show any coherent expansion pattern on large scale. And the nearby star forming region IC348 is supervirial but probably bound thanks to the gas mass (Cottaar et al. 2015).

For faraway regions that are barely resolved and for which  $\sigma_v$  cannot be measured, another diagnosis has been proposed by Gieles & Portegies-Zwart (2011). Noticing that all the stellar systems that stayed together for more than 30Myr and are most probably bound have an age that is larger than their crossing time  $t_{cr}$ , they suggest to use the ratio  $\pi = \text{age}/t_{cr}$  as a proxy to distinguish between clusters ( $\pi > 1$ ) and associations ( $\pi < 1$ ). However the  $\pi$  value is only indicative for regions younger than 10Myr and the distinction is not so clear.

For embedded regions, in which a lot of gas remains in particular, the differentiation between cluster and association is meaningless. Indeed a group that is bound thanks to the gas mass may become unbound after gas removal.

In this lecture, I will first present the properties of young stars in clusters (section 2), before describing how the global properties of open clusters can be used as probes of the galactic thin disk in section 3. I will then present the Gaia mission and discuss what we will learn from it in section 4.

## 2 Properties of stars in young clusters/associations

Young clusters and associations harbour homogeneous populations and represent ideal laboratories to study the properties of young stars and brown dwarfs in various environments with different ages and physical properties (e.g. density and/or metallicity).

### 2.1 *Census of the population*

#### 2.1.1 Membership criteria

In order to identify bona fide cluster/association members from observations, several criteria can be used. First of all, since they share the same age, metallicity and distance (for clusters only - for associations, individual parallax measurements are mandatory to take each star distance into account), their location in the HR diagram defines an isochrone whose color and luminosity can be used to distinguish members from field interlopers. Deep large scale photometric surveys in the optical, and then in the near-infrared to look for low mass objects and/or in extinguished regions, have been designed over the last twenty years for this purpose.

However, photometric data alone are not sufficient to distinguish cluster members since older but closer field stars may share the same properties. Complementary spectroscopic observations are thus often used to determine the candidate spectral types and/or to look for youth indicators such as the presence of lithium, a strong activity level or a low surface gravity.

Another powerful diagnosis is to look at kinematics (proper motion and radial velocity). Indeed, cluster or association members share the same space motion, with a velocity dispersion of the order of a few km/s, which offers an additional criterion to identify them. So far proper motion measurements from ground wide field imaging with a reasonable time baseline ( $< 10$  years) was only possible for fast moving ( $> 10$  mas/yr) groups. In some cases, like in Orion, the cluster momentum is roughly aligned with the line of sight and radial velocity obtained from high resolution spectroscopy may be the only way to disentangle young overlapping associations (e.g. OB1a, OB1b and 25 Ori; Jeffries et al. 2006, Briceño et al. 2007, Maxted et al. 2008, Sacco et al. 2008).

Bouy et al. (2013) recently developed a new astrometric pipeline able to combine and analyse archival data from various cameras at different telescopes to get a proper motion measurement accuracy better than 1 mas/yr (corresponding to 0.5 km/s at 100 pc). Thanks to Gaia, even more accurate astrometric data will soon become available, which is going to revolutionize our ability to derive membership from proper motion (see section 4). Astrometric measurements can also be used to determine the moving group convergent point (point in the sky towards which the velocity of all group members seems to point due to the projection on the celestial sphere) and constrain membership (Galli et al. 2012).

### 2.1.2 Membership analysis

Not so long ago, the usual way to search for members was to select candidates based on their photometric properties and then to do follow-up observations for each object to confirm its membership based on spectroscopy and/or kinematics. Over the last ten years, full sky proper motion catalogs such as PPMXL (Roeser et al. 2010) or UCAC4 (Zacharias et al. 2013) combining large photometric surveys have been available, and the use of astrometric data became more systematic to assess membership. Following the work of Sanders (1971), probabilities to belong to the group based on the are defined allowing to select only the most probable members. However, the contrast between the cluster population and the field decreases at fainter magnitudes as the proper motion measurement accuracy gets lower. Thus a single probability cut for all magnitudes is going to miss more low-mass members than high-mass ones and the level of contamination and/or incompleteness depends on luminosity. This has to be taken into account when studying the cluster population properties, but it is not always easy to estimate properly this bias.

New statistical methods (e.g. Sarro et al. 2014, Malo et al. 2013, Rizzuto et al. 2011) combining all the available informations (positions, proper motions, colors, and magnitudes) in a multi-dimensional analysis are being proposed to get self-consistent and robust membership probability whatever the object brightness. These Bayesian approaches can allow for a full treatment of uncertainties and missing data and may easily be extended to include other observables (like radial velocity, distance, rotation...), making obsolete the classical membership selection methods.

This methodology revolution is the consequence of the ever larger amount of more accurate and sensitive data with broader spatial, temporal and wavelength coverage that is becoming available. A good way to illustrate this is to look at recent studies made on the well-known Pleiades cluster. While Moraux et al. (2003) presented the results from a 6.4 square degrees imaging survey down to  $I \sim 22$  mag (which was one of the deepest and largest study in the Pleiades at that time), UKIDSS photometric data in five passbands as well as proper motion measurements for about 1 million sources spread over  $\sim 80$  deg<sup>2</sup> have been analyzed less than 10 years later (Lodieu et al. 2012). In the framework of the DANCe project<sup>1</sup>, Bouy et al. (2013) even increased the number of analyzed sources by a factor of about 3.5 and derived proper motions with an unprecedented accuracy (better than 1 mas/yr down to  $i \sim 23$  mag) by combining visible and near-infrared images obtained over 15 years from nine different instruments. Sarro et al. 2014 developed a new methodology to infer membership probabilities from this multi-dimensional data set in a consistent way, using a maximum-likelihood model using Bayes theorem. As a result, more than 2100 high-probability members have been identified, among which  $\sim 800$  are new (Bouy et al. 2015). These authors almost doubled the number of high probability members, and multiplied by five the number of substellar candidates, even though the Pleiades cluster had been intensively studied.

---

<sup>1</sup><http://project-dance.com>

## 2.2 IMF

One of the main motivations to obtain a full census of a cluster population is to derive its initial mass function (IMF) that corresponds to the distribution of stars at birth as a function of their mass, and to investigate its possible universality in a wide variety of environments. The IMF is an important physical property as its shape puts constraint on the star formation process and drives the evolution of clusters and galaxies. Several reviews of excellent quality have been published recently (Bastian et al. 2010, Jeffries 2012, Kroupa et al. 2013, Offner et al. 2014) and I refer the reader to these for more details.

### 2.2.1 Usual functional forms

There are usually three main functional forms used to describe the shape of the IMF:

- a power-law  $\chi(m) = \frac{dN}{dm} \propto m^{-\alpha}$  (or  $\phi(m) = \frac{dN}{d\log m} \propto m^{-\Gamma}$  with  $\alpha = \Gamma + 1$ ). This form has been first proposed by Salpeter (1955) with  $\alpha = 2.35$  (or  $\Gamma = 1.35$ ) for masses larger than  $1M_{\odot}$  and revised to a series of three segmented power-laws (Kroupa 2001) to represent the full mass range;
- a log-normal  $\phi(m) \propto \exp\left[-\frac{(\log m - \log m_c)^2}{2\sigma^2}\right]$  (Miller & Scalo 1979). More recently, Chabrier (2005) proposed a similar form up to  $1M_{\odot}$  but a Salpeter power-law at higher masses;
- and a tapered power-law  $\chi(m) \propto m^{-\alpha} \left[1 - e^{(-m/m_p)^{-\beta}}\right]$  (De Marchi et al. 2005).

But see also Cartwright & Whitworth (2012), Maschberger (2013), Basu et al. (2015) for alternatives.

### 2.2.2 IMF derivation

The methodology to compute the IMF of a resolved cluster consists in 1) determining the luminosity function (LF) of the sample of high-probability members and correct it from contamination, incompleteness and extinction when necessary; 2) converting the LF into a present day mass function (PDMF) using an evolutionary model; and 3) correcting the PDMF for stellar evolution and/or dynamical evolution to get the IMF.

The first step of this process is critical and great caution must be taken when dealing with a sample of cluster candidate members. Indeed, contamination of photometric surveys by field stars (dwarfs and giants) and extragalactic objects (galaxies, quasars) is always present whatever the method used for membership analysis. In principle, astrometric data should allow to reject most of the extragalactic sources as they are not moving but only if the mean cluster momentum is much larger than the measurement uncertainties. Incompleteness may also be

an issue if the survey does not extend beyond the cluster tidal radius, especially if there is mass segregation as the incompleteness level will then depend on mass. Moreover, objects might be missed around bright stars due to contrast issue, in crowded regions or in area with high extinction.

As for the second step, this is probably the one that suffers from the largest uncertainties. Indeed the conversion of colors and magnitudes into masses depends on evolutionary models which may not be very well constrained, especially at low masses and very young ages. As an example, the ONC mass function may show very different features below  $0.3M_{\odot}$  when using different models (see e.g. Da Rio et al. 2012). Moreover, even for the same set of models, the results may be very sensitive to the cluster estimated age or distance as shown by Scholz et al. (2013). For example, using an age of 1 Myr instead of 3 Myr for NGC1333 yields a different mass function. In addition to these model issues, individual stellar properties such as rotation rate and/or activity may influence the object luminosity and therefore the mass estimate. Indeed fast rotators may have a larger radius which would result in a larger luminosity and an overestimated mass. At the opposite, strong magnetic activity could create large cool spots which would reduce the effective temperature and underestimate the mass (see e.g. Mohanty et al. 2009, Stassun et al. 2014). The accretion history of a star could also affect its luminosity (up to  $\sim 10$  Myr, see Baraffe et al. 2009), and therefore its mass derivation, depending on how the star absorbs the accretion energy. And last but not least, multiple systems that are not resolved in the photometric images (typically for separations  $< 1$  arcsec, or  $< 100$  AU at 100 pc) are considered as single objects and their mass is therefore erroneous. If the effective temperature is used for conversion, then the obtained mass will be close but smaller than the real primary mass, but if instead the luminosity is used, the mass will be larger and actually closer to the total mass of the system. This means that even if using the same set of models, and the same age and distance, results may be different depending on how the conversion of the photometric properties into mass is performed.

The third and last step to derive an IMF is to correct the present day mass function from evolutionary effects. After a relaxation time  $t_{rlx} \sim (0.1N/\ln N)R/\sigma_v \sim (0.1N/\ln N)t_{cr}$  where  $N$  is the total number of cluster members and  $t_{cr}$  is the crossing time, enough exchanges of energy via 2-body interaction between cluster members have occurred to reach equipartition. This means in particular that lower mass objects have a higher velocity dispersion than more massive ones. As a consequence, mass segregation sets-up (the relative number of low mass stars with respect to high mass stars is smaller in the cluster center than in peripheric areas), and low mass members are lost preferentially by the cluster as a larger fraction of them have a velocity greater than the escape velocity. The latter effect can be clearly seen from observations: the Hyades PDMF (Bouvier et al. 2008) shows a clear deficit of brown dwarfs and low mass stars compared to that of the Pleiades, which is fully consistent with the dynamical evolution predicted by N-body simulations (see Figure 2). Consequently, the peak of the MF shifts towards higher masses as the cluster evolves, which has also been shown by De Marchi et al. (2010). For

a typical open cluster with  $R \sim 4$  pc,  $\sigma_v \sim 1$  km/s,  $M \sim 1000M_\odot$  and  $N \sim 2000$ , one has  $t_{cr} \sim 4$  Myr and  $t_{rlx} \sim 25t_{cr} \sim 100$  Myr. However, these values may change a lot from region to region. A denser cluster will evolve faster (as  $t_{cr}$  varies with  $1/\sqrt{\rho}$  where  $\rho$  is the cluster mean mass density), but so will a low- $N$  cluster ( $t_{rlx} \sim 2t_{cr}$  for  $N \sim 100$ ). It is important to keep in mind that a 10 Myr small group may be already relaxed and may have a PDMF that resembles that of a much older cluster. What really matters here is the age of the region with respect to its relaxation time.

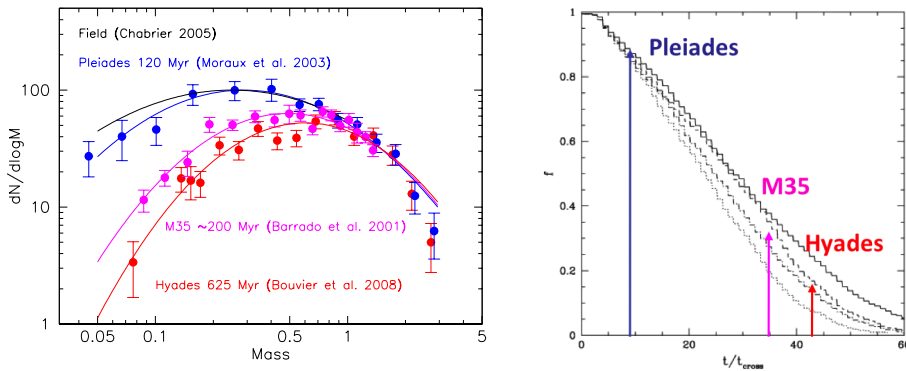


**Fig. 2.** *Left:* Present day mass function of three open clusters: the Pleiades (blue), M35 (magenta), and the Hyades (red). The field mass function from Chabrier (2005) is shown for comparison (black). *Right:* Results from N-body simulations showing the fraction of remaining brown dwarfs in the cluster as a function of age in crossing time unit (adapted from Adams et al. 2002).

Another strong limitation in the IMF derivation comes from stellar evolution that leads to the death of massive stars. Indeed the upper mass function cannot be directly determined from stellar counts above a given mass that depends on the age of the cluster, but has to rely on model.

In practice, most of the published PDMF are not corrected from the aforementioned evolutionary effects as it would add even more uncertainties in the IMF determination. It is important however to be aware of them and to look only at young and dynamically unevolved regions to be sure that the derived mass function is representative of the IMF.

### 2.2.3 IMF universality

In their review, Bastian et al. (2010) compiled a large number of young cluster and association mass functions to look for any possible variations of the IMF. Although each individual fit by a tapered power-law (see 2.2.1) yields different parameters, they conclude that there is no evidence for variation when comparing the IMF of



Milky Way stellar clusters as the observed differences are smaller than the uncertainties inherent to the mass function derivation (as described above). Dib (2014) made a thorough comparison of the mass function of eight young galactic clusters using Bayesian statistics. The IMF inter-cluster comparison shows that the parameters distributions do not overlap within the  $1\sigma$  level and the author concludes that the IMF is not universal. However, although the analyzed clusters have been chosen to reduce the uncertainties on the mass function derivation (i.e., only complete data have been taken into account and masses have been obtained using the same set of evolutionary models), they are still likely underestimated. The uncertainties on the cluster age and distance estimates are not taken into account, and the effects of rotation, magnetic activity and multiplicity are neglected. It is not possible to draw any conclusion on IMF variations until the cluster parameters have been ascertained and the models have been anchored at young ages and low masses. Hopefully, the situation should change soon thanks to the advent of Gaia.

One of the best constrained mass function to date is probably the Pleiades one since the cluster age ( $125 \pm 8$  Myr, Stauffer et al. 1998) and distance ( $130 \pm 10$  pc, Van Leeuwen 2009, Melis et al. 2014) are known with an accuracy better than 10%. The cluster is rich enough to minimize Poissonian errors and close enough to sample well into the substellar domain. The best lognormal fit to the *system* mass function in the  $[0.03 - 2]M_{\odot}$  range gives  $m_c = 0.25M_{\odot}$  and  $\sigma = 0.52$  (Moraux et al. 2003). Overlapping this fit to the mass function of a large number of open clusters and star forming regions reveals that they are all consistent within the uncertainties over the same mass range (see Offner et al. 2014, their Figure 2). Moreover, when considering three open clusters that have been analyzed in the exact same way by the same group (from the data reduction to the mass derivation and using data obtained with the same instrument and the same evolutionary models), their mass functions overlap almost perfectly and the best fit to the combined data gives  $m_c = 0.32_{-0.07}^{+0.08}M_{\odot}$  and  $\sigma = 0.52_{-0.09}^{+0.18}$  (see Figure 3). This suggests that the cluster stellar IMF may be universal, at least from  $0.03M_{\odot}$  to  $2M_{\odot}$ , and that a lognormal form may be a good representation in this mass range (see, however, Luhman et al. 2003 for Taurus).

Below  $0.03M_{\odot}$ , the situation is less clear. There may be some hint for variations as an excess of probable members between 0.01 and  $0.03 M_{\odot}$  has been claimed in Upper Sco (Lodieu et al. 2013) and in  $\sigma$ -Ori (Peña Ramírez et al. 2012). However, some issues remain regarding these results as most of the candidates still need to be confirmed spectroscopically and the mass-luminosity relation is very uncertain at such low masses. Future instruments such as the JWST will help to investigate the IMF in various regions at low masses and down to the planetary mass regime, to eventually search for a cut-off in the lower IMF.

Another way to look for IMF variations is to investigate very different environments in terms of density or metallicity. Young massive clusters in the Milky Way (see also the lecture from N. Bastian for extra-galactic ones) offer the possibility to look at the high mass part of the IMF which has been found to be flatter than Salpeter in some cases. This is in contradiction with recent estimate of the galactic disk IMF that is found to be steeper than Salpeter above  $1M_{\odot}$  with  $\alpha$  close to 3

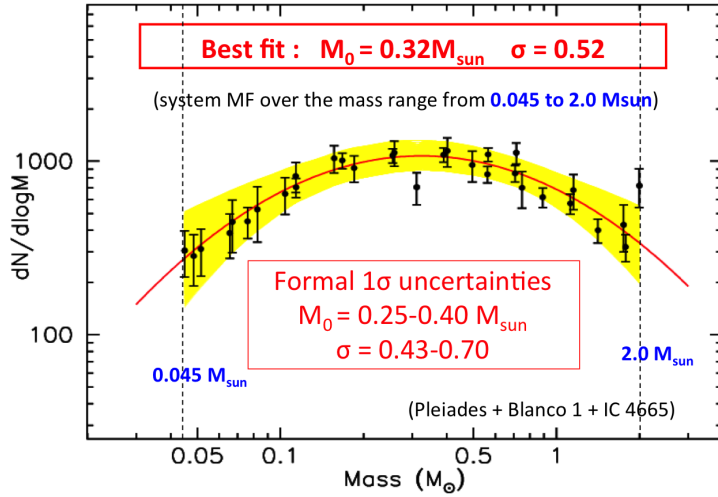


**Fig. 3.** Superimposed system mass function of three open clusters: the Pleiades (Moraux et al. 2003), Blanco 1 (Moraux et al. 2007), and IC4665 (De Wit et al. 2006). The red curve corresponds to the best lognormal fit to the combined data in the mass range  $[0.045\text{-}2] M_{\odot}$ , and the yellow area shows the  $1\sigma$  uncertainty of the fit.

(Czekaj et al. 2014). While the Arches mass function above  $1M_{\odot}$  is found to be consistent with a Salpeter IMF (Habibi et al. 2013), the Westerlund 1 one is controversial since Lim et al. (2013) report a flatter IMF while Gennaro et al. (2011) report a normal IMF. In the Quintuplet cluster, Hußmann et al. (2012) derived an IMF that is flatter than Salpeter, but this may be due to mass segregation as they only investigated the central part of the cluster. In the young nuclear cluster in the Galactic center, Lu et al. (2013) found a MF slope of  $\alpha = 1.7 \pm 0.2$ , which is again flatter than Salpeter. In NGC3603, the mass function is also a power-law with  $\alpha \sim 1.7$  but from  $0.4M_{\odot}$  to  $10M_{\odot}$  (Harayama et al. 2008, Stolte et al. 2006). No turnover has been found in this region yet, while there is one around  $0.5M_{\odot}$  in Tr14 (Rochau et al. 2011) and  $0.15M_{\odot}$  in Westerlund 1 (Andersen et al. 2016). The JWST and then the ELT will allow to refine these estimates and determine the IMF down to substellar masses in these regions.

In low metallicity environments, such as globular clusters (see C. Charbonnel’s lecture, and De Marchi et al. 2007) and the galactic bulge (Calamida et al. 2015), the IMF is found to be consistent with the lognormal shape proposed by Chabrier (2005) but the mass range probed by these studies is very narrow ( $0.2 - 0.8M_{\odot}$ ).

In conclusion, while the stellar IMF does not seem to vary significantly between  $0.03M_{\odot}$  and  $2M_{\odot}$  from region to region and appears to be independent of density, the situation is not as clear at lower masses nor at higher masses. In particular, departures from the Salpeter’s IMF have been found in young massive clusters and in the galactic disk but in the opposite direction. These possible variations

still have to be understood in the framework of star formation.

### 2.3 Multiplicity

Another ubiquitous outcome of star formation is stellar multiplicity. Characterizing the frequency and main characteristics of multiple systems and their dependencies on environment is therefore a powerful tool to probe this process. This could also help to correct the shape of the IMF from multiplicity and to disentangle features that may be due to multiplicity properties variations rather than to the individual star mass function. Duchêne & Kraus (2013) published a very complete review on stellar and substellar multiplicity in the field, but also in clusters and associations, and I refer the reader to it.

I will only focus here on the main difference between dense clusters and loose associations, namely the frequency of visual companions (separation between 10 to 3000 AU) that shows a clear dichotomy between these two kind of environments (see Duchêne & Kraus 2013, their Figure 4). The visual companion frequency observed in dense regions ( $> 50$  stars/pc<sup>2</sup>) is similar to that of field stars, but only about half that of low-density regions ( $< 10$  stars/pc<sup>2</sup>), whatever their age. For spectroscopic binaries however, no significant difference is observed whatever the regions.

This difference of visual companion frequency does not necessary imply that the initial multiplicity properties are environment-dependent however. Dynamical evolution may naturally explain both the low multiplicity and high multiplicity tracks, in which open clusters and loose associations represent extreme cases of highly effective and ineffective binary disruption respectively. Numerical simulations show that frequent interactions in dense clusters can reduce the initial multiplicity frequency by a factor of 2-4 within 1 Myr (e.g. Marks & Kroupa 2012). Current observations do not probe multiplicity in an early enough evolutionary stage to allow us to conclude on the universality of a high multiplicity frequency.

### 2.4 Substructures

It is clear from observations that open clusters and associations have a very different aspect: the former show a clear concentration of stars that can often be centrally defined, while the latter are spread over a large sky area. However, this difference is not so clear at very young ages. Indeed, Spitzer images have revealed that all embedded regions (bound or unbound) are substructured. High stellar concentrations are surrounded by a more extended population of young stars following the filamentary structure of the parent molecular cloud. Gutermuth et al. (2011) have shown that there is a strong correlation between the surface density of young stellar objects and the column density of gas. Some massive star forming regions exhibit large deviation from this correlation however as large stellar clusters are offset from high extinction area (e.g. CepOB2), but this may be due to gas dispersal by massive stars and non-coevality.

Recent multi-object high resolution studies indicate that substructures are also

present in the velocity space of young clusters (e.g. NGC2264, Fűrész et al. 2006) and are probably imprints of the formation history. Jeffries et al. (2014) identified two dynamically independent populations in Gamma Velorum: a virialized and centrally condensed group that could be a bound remnant of a dense cluster, and a supervirial, scattered population, spread over several degrees, older by 1-2 Myr, and further away by  $\sim 10$  pc.

Thus, being able to identify and characterize subgroups of young stars may shed light on the star formation process and help to understand the difference on the initial conditions that will lead to a cluster or an association. Cartwright & Whitworth (2004) defined a parameter  $Q$  to evaluate the degree of substructure that is based on the Minimum Spanning Tree (MST) algorithm (Gower & Ross 1969). It is defined as the ratio of the mean length of the tree branches to the normalized mean separation between stars. If  $Q > 0.8$ , the spatial distribution is smooth and centrally concentrated, substructured otherwise. The definition of a threshold for the MST branch lengths or the nearest-neighbor distances can also be used to identify groups (e.g. Gutermuth et al. 2009), in which the more massive stars tend to be towards the center.

Parker et al. (2014) performed N-body simulations of the dynamical evolution of substructured systems and found that subvirial initial conditions result in a global collapse that leads to a bound, centrally concentrated ( $Q > 0.8$ ) and mass segregated cluster within a crossing time (with  $t_{cross} \sim 1$  Myr). In contrast, if the initial conditions are supervirial, no global mixing occurs ( $Q$  remains small), the whole region expands and becomes an unbound association. These results suggest that clusters and associations may arise from the same star formation process but have a different dynamical evolution depending on the dynamical state of the region after gas removal.

### 3 Clusters as probes of the Galactic thin disk

Open clusters (hereafter OC) are powerful probes to characterise, study and analyse a variety of aspects related to the structure, composition, dynamics, formation and evolution of the Milky Way. Not being exhaustive, these aspects include:

- the Galactic spatial scales (scale height of the disk(s), height of the Sun above the Galactic plane, distance to the Galactic Centre) ;
- the spiral structure (tracing spiral arms) ;
- the kinematics and dynamics (rotation of spiral pattern, Galactic rotation curve, velocity of the local standard of rest, Oort constants, orbits of OCs and their relation to cluster survival/disruption) ;
- the Galactic formation and evolution (age of the oldest clusters, abundance pattern).

The main advantages of using open clusters is that they can be found at all ages and in a wide range of locations in the disk. Their parameters (age, distance, red-

dening) are available by, e.g., isochrone fitting of their colour-magnitude diagrams. Powerful statistical methods (e.g. Naylor & Jeffries 2006, Monteiro et al. 2010, Dias et al. 2012) have been developed yielding typical parameter uncertainties of the order of 5-10%.

There are also some disadvantages, or at least difficulties and systematics in studying the Galaxy on the basis of OCs. Confusion due to crowded backgrounds in the Galactic plane and dissolution of OCs introduce biases in the identification of clusters. These effects produce in particular selection effects against the low-mass OC that are faint and poorly populated, but also against old clusters, which are potentially poorer (due to dynamical evolution) than their younger counterparts. The extent of such a selection is far from being well known, but it must be kept in mind when deriving conclusions from the observed global properties of open clusters. Moreover, interstellar extinction affects the detectability of sources, introducing patterns in the distribution of open clusters that are often overlooked.

### 3.1 Catalogues

Using OCs for studying the Galaxy relies on a huge amount of data gathering and requires a catalogue of OC parameters (distances, ages, velocities, metallicities, diameters). Thousands of studies of individual OCs exist in the literature, often with nonconcordant results, mainly due to the variety of techniques to reduce data and derive parameters. This problem is well known and has motivated several attempts to derive homogeneous parameter sets.

In the 1980s, the Lund catalogue (Lynga 1982) contained around 1200 clusters, among which a few hundred had some of their parameters determined. A review on OCs and Galactic structure has been published by Janes & Adler (1982) and updated by Janes et al. (1988). The on-line WEBDA OC database (formerly BDA; Mermilliod 1992) appeared in the 1990s. More than a list of clusters with their parameters (essentially from the Lund catalogue), it included also actual measurements for their stars (photometry, astrometry, spectral types, etc.). From the observational point of view, CCDs and infrared arrays became of common use, and Hipparcos provided a wealth of astrometric and kinematic data and settled the distance scale through accurate parallaxes up to  $\sim 100$  pc. Although the new data did not bring significant results regarding the spatial structure of the Milky Way, the number of abundance measurements and discovery of older OCs shifted the focus on the origin and chemical evolution of the Galaxy. The main review on the subject is that of Friel (1995) and its updates. The 2000s brought the Dias et al. (2002) catalogue (DAML02) of optically revealed OCs, which updated the Lund catalogue.

All-sky proper-motion and photometric surveys have enabled the identification of OCs beyond simple visual recognition and opened the possibility to derive homogeneous data sets of Galactic clusters. Systematic searches for concentrations of stars at a common distance or with common proper motion, cluster sequences in CMDs or simply spatial concentrations of stars obeying some photometric criteria have allowed the discovery of several hundred optically vis-

ible OCs (e.g., Platais et al. 1998; Alessi et al. 2003; Kharchenko et al. 2005). Lists of infrared OCs and candidates have been compiled by Bica et al. (2003), Dutra et al. (2003), Froebrich et al. (2007, 2010), and Glushkova et al. (2010) based on 2MASS searches. These objects, detected in the near-IR, added about 700 clusters to the optically identified family. Taking advantage of more data becoming available, refined and homogeneous determinations of spatial, structural, kinematic, and astrophysical parameters for poorly studied clusters have been published (e.g. Bonatto et al. 2006; Piskunov et al. 2006; Kharchenko et al. 2009, Bukowiecki et al. 2011; Tadross et al. 2011; Kharchenko et al. 2013; Dias et al. 2014), and a number of clusters shown to be nonexistent have been removed from the catalogues. It is important to mention that distinguishing between true gravitationally bound, physical associations from chance aggregates on the sky requires in-depth follow-up for individual cluster candidates. The latest version (3.5) of the DAML02 catalogue<sup>2</sup> now includes  $\sim 2200$  clusters. 99.7% of them have estimates of their apparent diameters, and 92.4% have distance, reddening and age determinations. Concerning the kinematic data, 97.2% have their mean proper motions listed, and 43.1% their mean radial velocities. In total, 41.6% have distance, age, proper motion and radial velocity determinations simultaneously. Including IR discoveries, Kharchenko et al. (2013) published a list of  $\sim 2800$  open clusters called the Milky Way Star Clusters (MWSC) sample. They found that it is almost complete up to a distance of about 1.8 kpc from the Sun, except for the subset of the oldest open clusters ( $\log t > 9$ ), where there is evidence for incompleteness within 1 kpc from the Sun (Schmeja et al. 2014).

As for the total number of OCs in the Milky Way, estimates depend on many hypotheses, such as the variation of the clusters volume density with the distance from the Galactic Centre, or the cluster disruption rate. Recent studies indicate numbers on the order of  $10^5$  OCs (Bonatto et al. 2006; Piskunov et al. 2006).

### 3.2 Spatial distribution

Understanding the true shape of the Milky Way is a challenging task which depends essentially on the availability of complete Galactic surveys of the spatial distribution of stars, star clusters, molecular clouds, etc. The Milky Way is composed of the center and nuclear bulge, the thin disk hosting most of the OCs, the thick disk containing the old OCs, and the extended halo hosting old stars, white dwarfs and globular clusters (e.g. Majewski 1993). The gas and stellar density of the disk is usually expressed as a combination of exponential-decay profiles for the horizontal and vertical directions,  $\rho(r, z) \propto e^{(-r/R_D)}e^{(-|z|/z_h)}$ , where  $R_D$  is the scale length and  $z_h$  the scale height (e.g. Binney & Tremaine 1987).

Although the number of known OCs is small compared to stars, it is relatively simple and accurate to derive distance and age for these objects. In this sense, OCs may serve as a direct probe of the disk structure. Analysing a sample of 72 OCs Janes & Phelps (1994) found that the clusters younger than the Hyades (age

---

<sup>2</sup>The catalogue can be found on <http://www.wilton.unifei.edu.br/ocdb/>

(< 700 Myr) are strongly concentrated to the Galactic plane. They are distributed almost symmetrically around the Sun with a scale height perpendicular to the Galactic plane of  $z_h \sim 55$  pc. In contrast, the old OCs are more spread with  $z_h \sim 375$  pc.

The increased samples of OCs analysed in recent studies essentially recover this result, although in a clearer way. In particular, it is found that the disk scale height defined by the young clusters is smaller than that derived from older clusters, with the young and intermediate-age OCs (< 200 Myr versus < 1 Gyr) having scale heights of 48 pc and  $\sim 150$  pc, respectively (Bonatto et al. 2006). For older clusters, the vertical distribution is essentially uniform, so that no scale height can be derived. The average scale height, considering clusters of all ages, is  $z_h \sim 57 \pm 3$  pc (Bonatto et al. 2006; Piskunov et al. 2006). Also, the distribution of OCs younger than  $\sim 1$  Gyr clearly shows that  $z_h$  increases with Galactocentric distance, being about twice as large in regions outside the Solar circle than inside it (Bonatto et al. 2006).

Assuming that OCs are symmetrically distributed above and below the plane, the zero point of the height distribution gives a measure of the distance of the Sun from the Galactic plane. The current values determined from OCs range from about 15 to 22 pc (Bonatto et al. 2006; Piskunov et al. 2006; Joshi 2007; Buckner & Froebrich 2014).

The volume density of clusters in their plane of symmetry is 800-1000  $\text{kpc}^{-3}$  and the surface density is around 100-120  $\text{kpc}^{-2}$  for clusters closer than 1.8kpc (Kharchenko et al. 2013). The distribution of the surface density as a function of distance is almost flat, with a few exceptions. A significant excess of the youngest clusters at about 400 pc from the Sun is related to the Orion star formation complex. The surface density of the oldest clusters (>1 Gyr) presents a deficit below  $\sim 1.1$  kpc from the Sun, which may be due to incompleteness effects.

The interpretation for the above OC scale heights to be smaller than those attributed to the thin disk ( $z_h \sim 0.6$  kpc) as derived by means of stars (e.g. De Boer et al. 1997; Altmann et al. 2004; Kaempf et al. 2005) is not completely clear yet. This could be seen as a disk evolutionary effect, by which the disk would thicken with age due to some heating mechanism, or it could be an effect of the selective destruction of OCs that tend to be close to the plane. From the perspective of OCs seen as progenitors of the field population, Kroupa (2002) has shown that stars escaping the clusters, mainly during the process of gas dispersal, can thicken Galactic disks and even produce thick disks, which could also explain the scale height difference.

As for the the thicker scale height outside the solar circle, its precise meaning is not straightforward and is most likely a combination of effects such as the flaring of the disk and the amplitude of the warp.

### 3.3 *Spiral arms*

Although the spiral arm structure (see Fig. 4) in the Galactic disk is an important component when studying the morphology and dynamics of the Milky Way, a complete picture describing the nature, origin, and evolution of this structure

is still lacking. As recently suggested by Benjamin (2008), there may be two major spiral arms (Scutum-Centaurus and Perseus) with higher stellar densities and two minor arms (Sagittarius and Norma) mainly filled with gas and star forming regions. The nature of the Orion spur (or Local arm), i.e., the spiral feature inside which our Sun is located, has been elusive to present days. It might be a real arm, like Perseus, or a kind of inter-arm feature, like the ones seen in many external spirals.

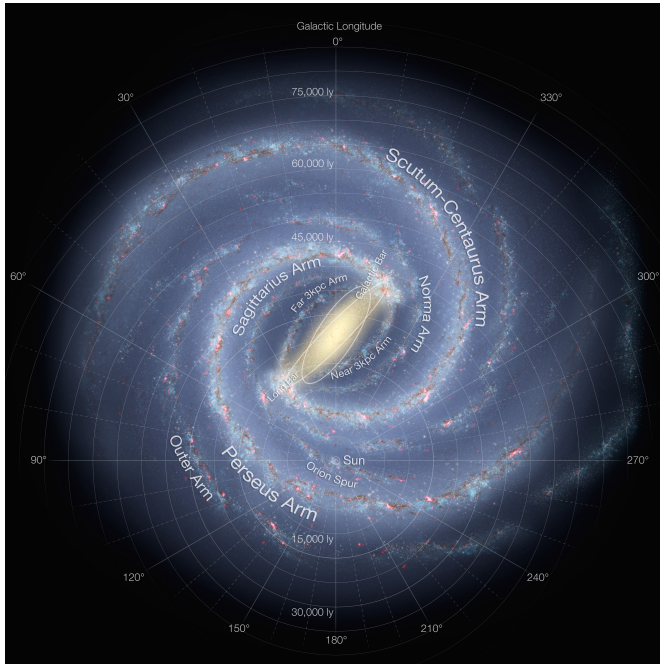


**Fig. 4.** Artist's view of the Milky Way (Credits: R. Hurt, NASA/JPL-Caltech/SSC)

Very young open clusters ( $<12$  Myr) and OB stars are powerful spiral arm tracers, and can probe spiral features in very remote regions of the Milky Way. At increasing cluster ages ( $12 < \text{age} < 20$  Myr), however, the spatial distributions get more scattered and no structure can be detected, since these clusters had a lot of time to move away from their birth-places (see Dias & Lépine 2005).

Historically, star clusters have been used to map the spiral structure of the Milky Way mainly in the third Galactic quadrant ( $180 < l < 270$  deg). In this area the extinction is small (Moitinho 2001) because the young disk is significantly warped (Moitinho et al. 2006), and star clusters can be detected to very distant regions (Carraro et al. 2010). A major breakthrough has been reported in Vázquez et al. (2008), where distances of a large sample of young open clusters (mostly from Moitinho 2001) are compared with CO clumps all the way to 20 kpc from the Galactic center in the anticenter direction.



This study indicates that the Perseus arm does not seem to continue in the third quadrant. Its structure is broken by the Local arm, which extends all the way to the outer, Norma Cygnus arm. If this is confirmed, it implies that the Local arm is a much larger structure than currently believed, and behaves like a bridge, connecting the Norma Cygnus arm in the outer disk possibly all the way to the Sagittarius arm in the inner first quadrant of the Galaxy. This picture of the Local arm as traced by young open clusters is in contrast with the GLIMPSE realization of the third quadrant, but in good agreement, e.g., with the HI study from Levine et al. (2006) who found a conspicuous Hydrogen structure departing from roughly the Sun location and entering the third quadrant, i.e., breaking Perseus and reaching the outer arm. It is therefore difficult to conceive that the Orion spur is a spiral arm like, e.g., Carina-Sagittarius or Scutum-Crux.

More recently, however, Xu et al. (2013) studied a sample of about 30 masers located in the Orion arm, and concluded that the kinematic of the sample is typical of a grand design spiral arm, and that the Orion spur is an arm of the same nature as Perseus or Scutum. Reid et al. (2014) published a substantial compilation of over 100 high-precision trigonometric distances to high-mass star forming regions using maser VLBI observations. Interestingly, they found that the Perseus arm, thought to be one of the major spiral arms of the Milky Way, has little massive star formation over a 6 kpc long arc between Galactic longitudes of 50 and 80 deg (Choi et al. 2014; Zhang et al. 2013). In contrast, the Local (Orion) arm has comparable massive star formation to its adjacent Sagittarius and Perseus arms.

### 3.4 Kinematics

The 1990s and 2000s witnessed a first explosion of astrometric data. The main results being the Hipparcos and Tycho-2 catalogues (ESA 1997; Høg et al. 2000), the UCAC2, 3 and 4 compilations, and the PPXML catalogue. However, while open clusters have often been used to investigate the local behaviour of the Galactic rotation curve, a proper rotation curve covering a sizable range of the Galaxy is still lacking. The outcome of most kinematic studies has been to improve the determination of parameters such as the local standard of rest (LSR) rotation speed corresponding to the circular orbital speed, the Oorts constants and the velocity of the Sun (e.g. Piskunov et al. 2006; Schönrich et al. 2010; Brunthaler et al. 2011; Bovy et al. 2012; Reid et al. 2014). The rotation curve is found to be flat between  $R_{GC} \sim 5$  and 15 kpc. The fundamental parameters of the Galaxy, including the distance of the Sun to the Galactic center,  $R_0$ , the circular orbital speed at the Sun,  $\Theta_0$ , and the solar motions with respect to the LSR, have been reevaluated to  $R_0 \sim 8.3$  kpc,  $\Theta_0 \sim 239$  km/s,  $U_\odot \sim 11.1$  km/s,  $V_\odot \sim 12.2$  km/s and  $W_\odot \sim 7.2$  km/s. These values are quite different from the IAU standards, which could have strong impact on our understanding of the Galaxy. For example, increasing  $\Theta_0$  by 20 km/s would result in a 30% increase in the estimate of the mass of the Milky Way (dark-matter dominated).

In addition to these calculations, OCs have also been used recently to determine the rotation speed of the spiral pattern. Dias & Lépine (2005) confirmed that

spiral arms rotate as rigid bodies, and determined the pattern speed by direct integration of cluster orbits and by comparing the positions of clusters in different age groups, leading to an adopted value of 24 km/s/kpc. As an additional result, they found that the corotation radius is  $(1.06 \pm 0.08) \times$  the solar Galactocentric distance. It is also interesting to note that Bobylev et al. (2007) found a different speed for the Orion arm compared to Carina-Sagittarius and Perseus. Another basic parameter is the epicyclic frequency (the circular velocity obtained after subtracting the Galactic rotation curve) which Lépine et al. (2008) found to be  $42 \pm 4$  km/s/kpc at the solar radius.

### 3.5 *Metallicity distribution*

Open clusters, found at all ages and throughout the Galactic disk, serve as excellent tracers of the overall chemical enrichment of the disk. As they preserve the abundances of the gas from which they formed, studying the chemical profiles of clusters of different ages and locations provides the history of star formation and nucleosynthesis throughout the galaxy and across its lifetime. Recent high precision analyses indicate that stellar abundances among cluster members are highly uniform, consistent with no intrinsic scatter within the cluster (De Silva et al. 2006), so one can be assured that the determined abundances reflect the initial composition in a well-mixed gas cloud.

The study of the radial metallicity distribution through open clusters sees the first pioneering work at the end of the 70s, when Janes (1979), using the photometric metallicity determination of about 40 clusters located within 6 kpc from the Sun, derived for the first time, a radial gradient of  $[\text{Fe}/\text{H}]$ . They found that metallicity decreases from the inner to the outer parts of the Galaxy at a rate  $d[\text{Fe}/\text{H}]/dR = -0.05$  dex/kpc. During the following decades, many authors have tackled the argument, using gradually more accurate determination of the cluster parameters, and, especially, of their metallicity through low, medium and finally high resolution spectroscopy. A non-exhaustive list of works dedicated to the study of the Galactic metallicity gradient with open clusters includes Friel (1995), Friel et al. (2002), Yong et al. (2005), Sestito et al. (2006, 2008), Pancino et al. (2010), Yong et al. (2012), Heiter et al. (2014). The most common results are linear fits over the complete investigated galactocentric radius ( $R_{GC}$ ) range or gradients with different slopes for inner and outer areas. While the inner disk ( $< 10$  kpc) shows a steep gradient, the metallicity distribution of the outer area is almost flat. Twarog et al. (1997), or more recently Lépine et al. (2011), provided however another interpretation of the radial metallicity distribution with two shallow plateaus and a step of  $\sim 0.3$  dex at  $R_{GC} \sim 9$  kpc. Lépine et al. (2011) explained this as a consequence of the corotation ring-shaped gap in the density of gas and that the metallicity evolved independently on both sides.

Numerous studies have been devoted to understanding how the evolution of the Milky Way shaped this chemical gradient (e.g. Chiappini et al. 2001; Cescutti et al. 2007; Magrini et al. 2009; Lépine et al. 2011). Various physical processes are responsible for the observed distribution of elements in the Milky Way disk. Chem-

ical evolution models explore the influence of star formation rates, recycling of material processed by the stars, infall rates of extragalactic material onto the disk, and the variation of those quantities with Galactocentric radius to determine the combination that best reproduces the shape of the gradient at various epochs. Recent works based on chemodynamical simulations (Roškar et al. 2008; Minchev et al. 2013, 2014) take into account stellar migration, and the fact that the present-day Galactocentric radius of a tracer may be different from its birth radius.

Large samples including clusters of different ages allowed to deal with the temporal variation of the radial gradient (e.g., Chen et al. 2003; Magrini et al. 2009; Jacobson et al. 2011; Andreuzzi et al. 2011; Frinchaboy et al. 2013). Netopil et al. (2016) found that the older clusters ( $\sim 1.7$  Gyr) appear more metal rich by about 0.07 dex than young clusters ( $< 0.5$  Gyr). This is clearly the opposite of what was commonly looked for in the past, i.e., a decline of metallicity with cluster's age, but it might be an observational confirmation of radial migration. However, to further validate this result, a homogeneous age scale for the clusters and a somewhat larger sample of older systems are needed.

Taking all together, the literature results can be summarised as:

- the global , i.e., including clusters of all ages, radial metallicity distribution traced by open clusters shows a steep inner gradient of -0.09 to -0.20 dex/kpc out to  $R_{GC} \sim 10-12$  kpc, and then presents either a shallow gradient or a plateau at  $\sim -0.3$  to  $-0.5$  dex from the breaking radius to the most faraway clusters, i.e.,  $R_{GC} \sim 20-23$  kpc;
- there is a notable dispersion in metallicity at any Galactocentric distance, typically of  $\sim 0.5$  dex;
- concerning the time evolution of the gradient, there is a suggestion that younger clusters follow a flatter gradient than older clusters up to the breaking radius. However, due to the small number of clusters in different age bins, the slopes of the gradient at different ages are sensitive to the binning and to the definition of the position of the breaking radius (cf., e.g., Magrini et al. 2009, Jacobson et al. 2011).

While overall metallicity and Fe abundances are useful in tracing the general trends of chemical enrichment, the details of star formation and nucleosynthesis are revealed in the behavior of elements such as oxygen and the  $\alpha$ -elements Mg, Si, Ca, and Ti, and their specific abundance pattern. These elements are formed through stellar nucleosynthetic processes in massive stars, and, as a result, are quickly recycled to the interstellar medium through mass loss and Type II supernovae explosions. Elevated abundances of these elements, relative to the solar ratios, point to episodes of rapid star formation and distinctive star formation histories.

Several groups (e.g., Bragaglia & Tosi 2006 and the Bologna Open Cluster Chemical Evolution project; Sestito et al. 2008; Carraro et al. 2007; Jacobson et al. 2009; Friel et al. (2010); Yong et al. 2005) have led the effort in characterizing the clusters chemical patterns. Although limited by small statistics, results indicate that

groups of clusters located at similar  $R_{GC}$  share similar chemical patterns in general, but remarkable differences are seen for some abundance ratios in some clusters (Magrini et al. 2014).

### 3.6 Age distribution

The distribution of cluster ages sheds light on the balance between cluster formation and disruption. If the cluster population seen today were the result of a uniform formation rate combined with an exponentially declining dissolution rate, one would expect to see a simple exponential distribution with a characteristic single lifetime. What is seen is much different. The age distribution of clusters shows three distinct populations with different timescales of longevity.

The youngest cluster population has a lifetime of only a few tens of millions of years or less. A group of such young clusters is apparent in any large sample, and their numbers rapidly decrease with age beyond  $\sim 10$  Myr. These systems are stellar associations that are not gravitationally bound, and are in the process of dissolving and dispersing into the general field population. Dissolution here occurs mainly because the gravitational potential can be rapidly reduced by the impulsive gas removal by supernovae explosions and massive star winds associated with this early period. Thus, a significant fraction of the stars end up moving faster than the scaled-down escape velocity, and may escape into the field (e.g., Goodwin & Bastian 2006).

Most of the clusters have a characteristic lifetime of a few hundred million years and represent a rather homogeneous group. This population dominates the Galactic system of open clusters and largely defines the properties of the typical open cluster. The exponential decay time for these clusters has been found to be between  $\sim 120$  and  $320$  Myr (e.g., Bonatto et al. 2006; Piskunov et al. 2006). The cluster disruption timescale varies with mass as  $t_{dis} \sim M^{0.62}$  (e.g. Lamers & Gieles 2006), which means that solar neighbourhood clusters with mass in the range  $10^2 - 10^3 M_{\odot}$  dissolve on a timescale  $75 < t_{dis} < 300$  Myr. This occurs because OCs continually undergo mass segregation and evaporation, tidal interactions with Galactic substructures, shocks with giant molecular clouds, as well as mass-loss due to stellar evolution. By decreasing the total cluster mass and the collective gravitational potential, these processes affect the internal dynamics and accelerate the cluster dynamical evolution until dissolution in the Galactic stellar field.

Nevertheless, as was first apparent in Janes et al. (1988) and reinforced with larger samples in Janes & Phelps (1994), the age distribution shows a long tail to larger ages, in a distribution that cannot be fitted by a single exponential with a decay time of a few hundred million years. This third group represents only a few percent of the total cluster population and includes members with ages approaching the age of the Galactic disk, that can be characterized with lifetimes of 3-4 Gyrs. Janes & Phelps (1994) fit this older population in the cluster age distribution with an exponential of 3-5 Gyrs, while Bonatto et al. (2006) derived an exponential timescale of  $2.4 \pm 1$  Gyr for this old population. In either case, there is a substantial population of old clusters not explained by the simple picture

of uniform formation rate combined with dissolution.

The mix and relative numbers of these populations vary with location in the Galaxy, leading to the spatial distribution correlating with age. The outer disk clusters are systematically longer lived and survive about twice as long as a typical open cluster in the inner disk. The characteristic lifetime of open clusters of all types seems to be a distinct function of galactocentric radius (Friel 2013).

### 3.7 Cluster mass function

Although being a basic parameter for the study of cluster evolution, the total mass  $M_c$  of an open cluster can not be derived directly from the observations. Indirect methods require, however, a number of assumptions that can cause different biases in the resulting mass estimates.

There are at least three independent methods for estimating cluster masses, each with advantages and shortcomings. The simplest and most straightforward way is to count cluster members and to sum up their masses. This is however challenging as it requires a complete census of cluster members from the low mass objects to the highest mass stars, and from the central parts to the outskirts of the clusters. Incompleteness may arise from either the limiting magnitude or the limited field of view or both. Moreover the conversion from luminosity to mass relies on evolutionary models that may not be very well constrained, especially a very young ages.

Another independent method is based on the virial theorem: the mass of a cluster is determined from the 3-D stellar velocity dispersion  $\sigma_v$  using the relation  $M_c = R_g \sigma_v^2 / G$ , where  $R_g$  is the cluster gravitational radius. This does not require the membership determination of all cluster members but the above relation assumes that the cluster is virialized which may not be the case, especially for young cluster. Moreover, the gravitational radius  $R_g$  is obtained by fitting the cluster density profile (which may not be spherical however), and may be underestimated if mass segregation is present. The estimate of  $\sigma_v$  is not an easy task either as the typical velocity dispersion of open clusters is  $\sim 1$  km/s, and may be biased by the presence of binaries.

The third method uses the interpretation of the tidal interaction of a cluster with the parent galaxy, and requires knowledge of the tidal radius  $r_t$  of a cluster. It gives the so-called ‘‘tidal mass’’  $M_c = \frac{4A(A-B)r_t^3}{G}$  (King 1962) where A and B are the Oort constants. The tidal radius is usually obtained from a three-parameter fit of a King profile to the cluster member surface density distribution. This method assumes systems with spherical density distributions whereas open clusters can have irregular or elliptical shape. Another possible bias in the resulting tidal radius may arise from the magnitude limit and/or the restricted covered area used to build the cluster star sample from which the density profile is built. This effect is particularly important for distant or mass segregated clusters, for which the tidal radius may easily be wrong by a factor of 2, and the mass by a factor of 8 as it varies with  $r_t$  cubed. Tidal masses are, on average, larger than masses

obtained exclusively from star counts.

Whatever the method, the cluster present day mass function (CPDMF), i.e., the mass distribution of Galactic open clusters, is found to extend from  $\sim 100$  to  $10^6 M_\odot$  and the high-mass part of the CPDMF ( $> 10^3 M_\odot$ ) follows a power-law  $dN/dM_c \propto M_c^{-\alpha}$  with  $\alpha \sim 2.0 - 2.2$ . This exponent increases with age as a direct consequence of the mass-loss of clusters due to dynamical evolution. When taking into account only the youngest clusters with age  $< 10$  Myr,  $\alpha$  is found to be around  $1.7 - 2.0$  (e.g. Piskunov et al. 2008). This result is consistent with the embedded-cluster mass function that follows a power law with a similar exponent (e.g. Lada & Lada 2003).

### 3.8 Star formation rate in clusters

Looking at the cluster age distribution, it appears that there has been a local starburst between 220 and 600 Myr and that the star formation rate (SFR) in the solar neighborhood is not constant. The SFR is found to be around  $4800 M_\odot/\text{Myr}$  during this period while it is around half for the rest of the time (Bonatto & Bica 2011). There seems also to be an excess of young clusters ( $< 9$  Myr), and the obtained SFR in these young clusters is similar to the one derived for embedded clusters, indicating that a majority of stars ( $> 80 - 90\%$ ) form in groups. However, many of these systems may not be bound and could instead be associations in the process of dissolving. Indeed, only a fraction of  $\sim 10\%$  survive the first 10 Myr (Lada & Lada 2003) suggesting that only a minority of field stars were born in groups that were massive enough to become open clusters.

However, recent results on the multiplicity properties of field stars (Duchêne & Kraus 2013), suggest that most of them cannot come from loose associations either, as the observed visual companion fraction (separation between 10 to 3000 AU, see section 2.3) is much lower in the field compared to these regions. Therefore, most of the thin disk population seems to originate from intermediate regions, that are dense enough to process visual binaries but not massive enough to survive the first 10 Myr after gas removal.

## 4 What will we learn from Gaia?

### 4.1 The Gaia mission

The Gaia satellite<sup>3</sup> is a European Space Agency (ESA) cornerstone project, aimed at understanding how our Milky Way galaxy was formed and how it has evolved into what it is today. Gaia was selected by ESA in 2001 and launched on 19 December 2013 from Kourou (French Guiana) with a Soyuz-Fregat rocket. It was put on a Lissajous orbit around L2, 1.5 million km away from the Sun, for an expected five year lifetime of operations, with a possible extension of one year.

---

<sup>3</sup><http://www.cosmos.esa.int/gaia>

Gaia has been designed to measure star positions with extreme accuracy (see Perryman et al. 2001). It will perform an all sky survey complete to  $G \sim 20.7$ , corresponding to  $V \sim 20 - 22$  mag for blue and red objects respectively, obtaining astrometric data with micro arcsec ( $\mu\text{as}$ ) accuracy for more than a billion stars, as well as optical spectrophotometry for most of them, and medium resolution spectroscopy at the Ca II triplet (847-870 nm) for several million objects brighter than 16th mag. It is the successor to the Hipparcos mission, the first precision-astrometry space mission, which produced a catalog of positions, parallaxes and proper motions for about 100,000 stars. Gaia will take this further by targeting  $10^4$  more stars across the Milky Way, and with an astrometric accuracy  $\sim 100$  times better. It will provide in particular one-percent accurate distance for 10 million stars (while it is the case for only seven hundreds stars today).

#### 4.1.1 Payload and instruments

Global astrometry requires repeated observations of the same area of the sky from two lines of sight separated by a suitable and very stable angle. For this purpose, Gaia's payload carries two identical telescopes (each holding a  $1.45\text{m} \times 0.5\text{m}$  rectangular mirror), pointing in two directions separated by a 106.5 degree basic angle and merged into a common path in the focal plane. The satellite spins around its axis, which is oriented 45 degrees away from the Sun, with a period of 6 hours, and the spin axis has a precession motion around the solar direction with a period of 63 days. The combination of these two motions results in a quasi-regular time-sampling that allows to scan the entire sky on average 70 times over the 5 year mission lifetime, with more than 200 transits in a  $\sim 10$  degree strip at 45 degree latitude above or below the ecliptic plane, and as little as  $\sim 50$  transits in other areas of the sky (see Figure 5).

The Gaia focal-plane assembly is the largest ever developed for a space application, with 106 CCDs of  $4500 \times 1966$  pixels, yielding a total of almost 1,000 million pixels of  $10 \times 30 \mu\text{m}^2$ , and a physical dimension of  $1.0\text{m} \times 0.4\text{m}$ . It serves five main functions:

- the wave-front sensor (WFS) and basic-angle monitor (BAM);
- the Sky Mapper (SM), autonomously detecting objects entering the fields of view and communicating details of the star transits to the subsequent CCDs;
- the main Astrometric Field (AF), composed of 62 CCDs with a field of view of  $40 \times 40$  arcmin on the sky, devoted to astrometric measurements and  $G$ -band (330-1050 nm) photometry;
- the Blue and Red Photometers (BP and RP), providing low resolution ( $R < 100$ ) slitless spectrophotometry for each object over the wavelength ranges 330-680 and 640-1000 nm, respectively, as well as integrated  $G_{BP}$  and  $G_{RP}$  magnitudes (and colour);

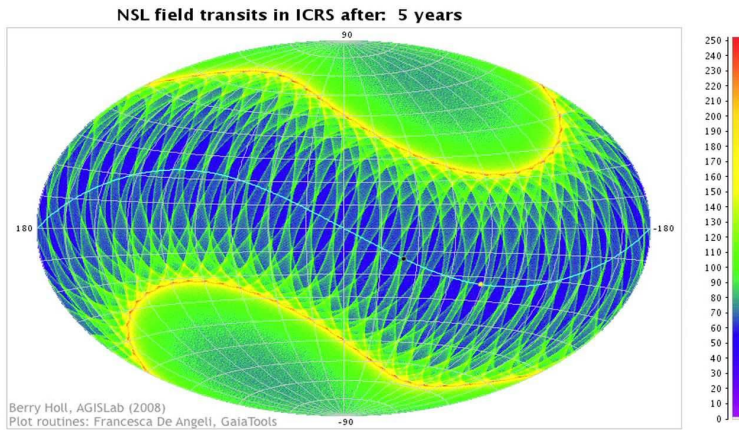


**Fig. 5.** Gaia nominal skying law. The color scale indicates the number of Gaia visits on the sky in equatorial (ICRS) coordinates after 5 years. The light blue line corresponds to the ecliptic plane.

- and the Radial-Velocity Spectrometer (RVS), registering slitless spectroscopy at the Ca II triplet (845-872 nm) with  $R \sim 11,500$  brighter than  $G \sim 16$  mag.

Measurements are made in time-delayed-integration (TDI) mode, reading the CCDs at the same speed as the sources trail across the focal plane, i.e., 1 arcmin/sec, corresponding to a crossing/reading time of 4.4 sec per CCD. Since Gaia observes objects over a very wide range of apparent magnitude, the CCDs must be capable of handling a wide dynamic signal range. A number of features have been incorporated in the CCD design in order to cope with bright stars. These include a large full-well capacity, an anti-blooming drain, and TDI gates which effectively reduce the integration time for bright objects.

The Gaia CCD detectors feature a pixel size of  $10 \mu\text{m}$  (59 milli-arcsecond) in the scanning direction and the astrometric instrument has been designed to cope with object densities up to 750,000 stars per square degree. In denser areas, only the brightest stars are observed and the completeness limit will be brighter than 20th magnitude.

#### 4.1.2 Science performance

The commissioning phase was completed on 18 July 2014. The overall performance was assessed to be very good, and the detection efficiency was improved so as to extend the bright end to  $G \sim 0$  mag through detection algorithm improvements and employment of a special observing mode. The faint limit was also extended down to  $G = 20.7$  mag. However, a few problems were identified: stray light (mostly due to scattering from filaments on sunshield edges), contamination (thin ice layer on optics), and some larger than expected variations of the basic angle.



These effects can be mitigated (e.g. by periodic decontamination campaigns) or modelled, and actions have been taken to this purpose. Updated performances can be found on the ESA website in the Gaia performance pages <sup>4</sup>. They are summarized below.

**Astrometry** In order to get the five standard astrometric parameters, position ( $\alpha$ ,  $\delta$ ), parallax ( $\pi$ ), and proper motion ( $\mu_\alpha$ ,  $\mu_\delta$ ) for all observed objects brighter than  $G = 20.7$  mag with micro-arcsec accuracy, all the available  $\sim 70$  observations per object gathered during Gaia's 5 year lifetime will have to be combined in a single, global, and self-consistent manner. While a daily data treatment is performed to estimate source positions, satellite attitude and calibration parameters at the level of sub-milli-arcsec accuracy, the Astrometric Global Iterative Solution (AGIS) system is run about every 6 months on an ever increasing data volume. AGIS treats the wanted source parameters, the satellites attitude and calibration parameters as unknowns and tries to find iteratively the best global match in a least-square sense between all measurement data and an observational model that is formulated in terms of these unknowns. This is the reason why Gaia is sometimes referred to as a self-calibrating mission. Only single, non-variable stars which fit the standard 5-parameter astrometric model will take part in such a primary AGIS cycle. For the remaining objects (binary, multiple systems, etc.) only provisional values will be computed by AGIS in a subsequent secondary cycle which optimizes source parameters using the attitude and calibration solutions from the preceding primary cycle.

Taking into account all the known instrumental effects (except the slow optics contamination by thin ice which is expected to remain small) under the appropriate in-flight operating conditions plus a 20% science margin <sup>5</sup>, the predicted end-of-mission parallax standard error  $\sigma_\pi$  is shown on Figure 6 for a single unreddened G2V star. All error sources have been included as random variables with typical deviations (as opposed to best-case or worst-case deviations). The behaviour of the curves clearly shows two regimes: the bright star regime ( $G < 12$ ) where performance is set by bright-star centroiding and calibration errors, and the faint star regime ( $G > 12$ ) where photon-noise dominates.

Using scanning law simulations, the sky-averaged position and proper-motion errors,  $\sigma_0$  [ $\mu\text{as}$ ] and  $\sigma_\mu$  [ $\mu\text{as}/\text{yr}$ ] can be deduced from  $\sigma_\pi$  [ $\mu\text{as}$ ] using the following relations:

$$\sigma_0 = 0.743 \sigma_\pi$$

$$\sigma_\mu = 0.526 \sigma_\pi$$

Knowing that a star transverse velocity in km/s is given by  $V_T = 4.74\mu/\pi$ , with  $\mu$  the star annual proper motion and  $\pi$  its parallax, the uncertainty on the transverse velocity  $\sigma_{V_T}$  can easily be derived from  $\sigma_\pi$  and  $\sigma_\mu$ . It is shown in Figure 7 as

<sup>4</sup><http://www.cosmos.esa.int/web/gaia/science-performance>

<sup>5</sup>see <http://www.cosmos.esa.int/web/gaia/science-performance> for more details about this science margin

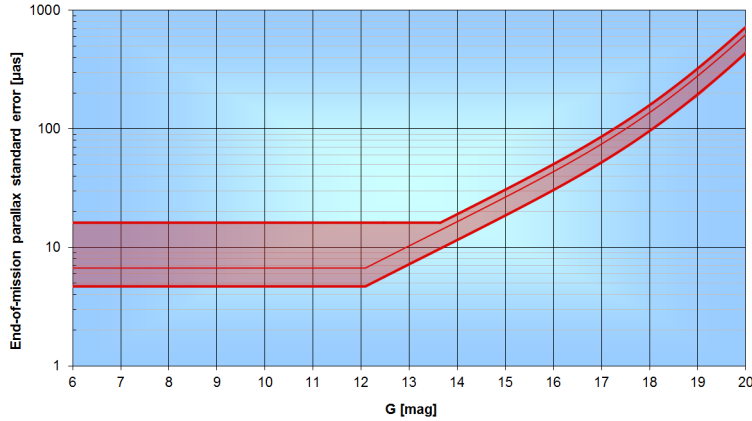


**Fig. 6.** Sky-average end-of-mission parallax standard error, in  $\mu\text{as}$ , as function of Gaia  $G$  magnitude for an unreddened G2V star ( $V - I = 0.75$  mag,  $V - G = 0.16$  mag). The upper and lower curves reflect the range resulting from varying the sky position, the  $V - I$  colour index, and the bright-star (TDI-gate) observing strategy. Figure taken from the Gaia performance pages.

a function of the  $G$ -band magnitude. In this diagram, slope discontinuities appear first at  $G = 12$ , resulting from the constant bright-star parallax accuracy adopted for  $G < 12$ , and then at different magnitudes when the distance is equal to 2.4 kpc, i.e., when the Galactic shearing takes over on the random velocity dispersion.

**Photometry** Gaia’s photometry comprises: broad-band  $G$ -band fluxes obtained from the astrometric instrument, and low-resolution spectro-photometry obtained from the Blue (330-680 nm) and Red (640-1050) Photometers (BP and RP). The wavelength coverage of the astrometric instrument defining the  $G$ -band is  $\sim 330$ -1050 nm. The Sloan/Cousins/Johnson magnitude/colour transformations presented in Jordi et al. (2010) allow estimation of the broad-band Gaia  $G$ -magnitude as a function of  $V$  and  $V - I_C$ . The spectral dispersion of the photometric instrument is a function of wavelength and varies from 3 to 27 nm/pixel in BP and from 7 to 15 nm/pixel in RP. Whereas the  $G$ -band data are particularly useful for stellar variability studies, the BP/RP spectra allow to classify sources and to determine their astrophysical parameters, such as interstellar extinction, surface gravity, effective temperature, etc. Bailer-Jones et al. (2013) have shown that for FGKM stars with magnitude  $G = 15$  (i.e.,  $V \sim 15 - 17$  depending on the source colour), the effective temperature can be estimated to within  $\sim 100$  K, the extinction  $A_V$  to  $\sim 0.1$  mag, the surface gravity to 0.25 dex, and the metallicity  $[\text{Fe}/\text{H}]$  to 0.2 dex, using just the BP/RP spectro-photometry. They found that

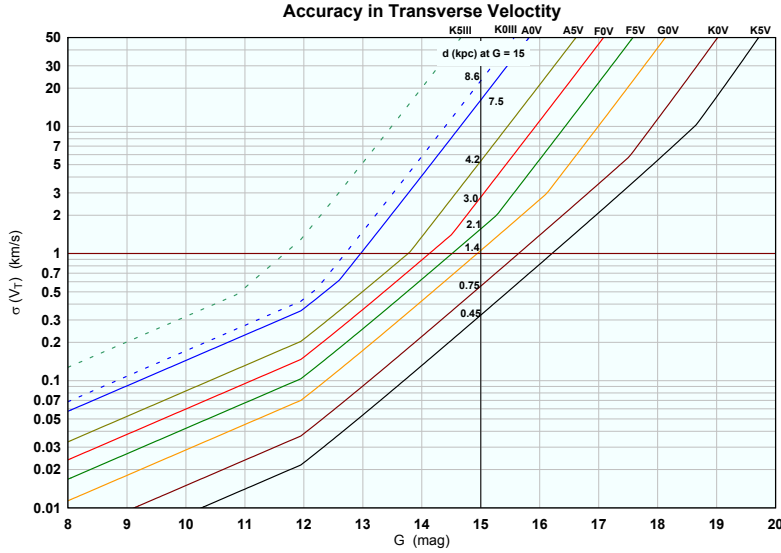


**Fig. 7.** Expected performance of Gaia in the determination of the transverse velocity for a sample of representative stars, as a function of the magnitude in the Gaia broad band (the  $G$  magnitude). The uncertainties are determined from a combination of the uncertainties in the annual proper motion and parallax, as a function of the  $G$  magnitude (from F. Mignard, GAIA-CA-TN-OCA-FM-048-1 technical note).

the accuracy of these estimates depends on the  $G$  magnitude and on the value of the stellar parameters themselves, and may vary by a factor of more than two up or down over this parameter range. These performances are based on pre-launch simulations and would need to be confirmed on real data.

**Spectroscopy** Among the myriad of data collected by the ESA Gaia satellite, about 150 million high-resolution spectra will be delivered by the Radial Velocity Spectrometer (RVS) for stars as faint as  $G_{RVS} \sim 16$  mag.

Radial velocities are the main product of the RVS, allowing to complete the five standard astrometric parameters obtained by the Astrometric Field (AF) and obtain a 6-D view (in the position and velocity phase-space) of the galactic stellar population. The calculation methodology prescribes that a single end-of-mission composite spectrum is reconstructed by co-addition of all spectra collected during the five-year mission, and an average radial velocity is then extracted by cross correlation with a template spectrum. Typical end-of-mission errors are 1 km/s at  $V \sim 7.5$ , 12.3, and 15 km/s at  $V \sim 11.3$ , 15.2 for a B1V and G2V star respectively (see Figure 8). Whenever possible, an *a posteriori* on-ground data analysis will be done to derive also single epoch radial velocities.

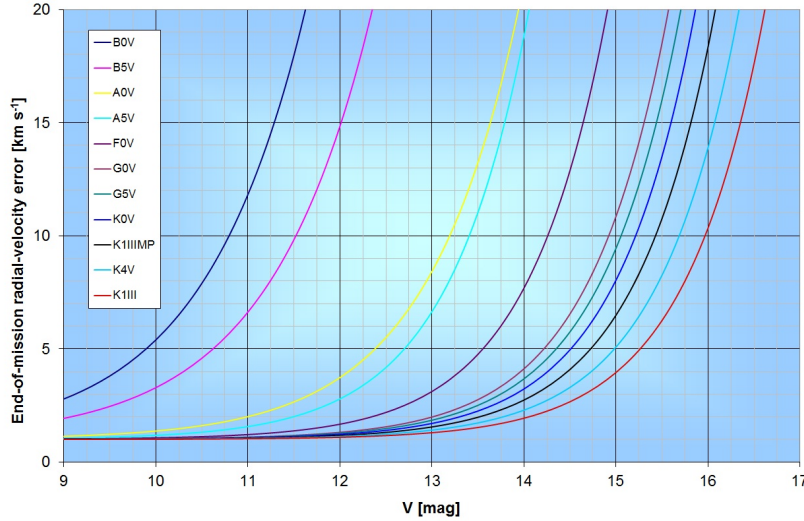


**Fig. 8.** Expected RVS performance for a sample of representative stars, as a function of their  $V$  magnitude. Plot available in the Gaia Performance Pages.

By comparison to the expected performance in transverse velocity plotted in Figure 7, one can see that globally the radial velocity accuracy for G to K stars around  $V = 15 - 16$  (corresponding to the core of the Gaia mission), is smaller but only by a factor of a few. For fainter stars, the RVS performance degrades much faster than the astrometric determination of the transverse velocity and at the faint end, there is no radial velocity measurement at all. For stars brighter than  $V \sim 13$ , the RVS performance remains rather constant, close to 1 km/s, while the expected transverse velocity accuracy is much better, typically by one order of magnitude. Complementary ground based observations are thus necessary to improve the radial velocity accuracy at the level of the transverse velocity, a desirable feature for kinematic studies.

In addition to radial velocity measurements, a specific stellar characterization will be performed on single star RVS spectra with high enough signal-to-noise ratio ( $G_{RVS} < 14.5$  mag), and some individual chemical abundances will be estimated for the brightest targets ( $G_{RVS} < 11$  mag,  $\sim 2$  million stars). A recent study from Recio-Blanco et al. (2016) indicate that stars brighter than  $G_{RVS} \sim 12.5$  are efficiently characterized, with reliable estimations of  $[\alpha/\text{Fe}]$ . Typical internal errors for FGK stars are around 40 K in  $T_{eff}$ , 0.10 dex in  $\log(g)$ , 0.04 dex in  $[\text{M}/\text{H}]$ , and 0.03 dex in  $[\alpha/\text{Fe}]$  at  $G_{RVS} = 10.3$ . They degrade to 155 K in  $T_{eff}$ , 0.15 dex in  $\log(g)$ , 0.10 dex in  $[\text{M}/\text{H}]$ , and 0.1 dex in  $[\alpha/\text{Fe}]$  at  $G_{RVS} \sim 12$ . Similar accuracies in  $T_{eff}$  and  $[\text{M}/\text{H}]$  are found for A-type stars, while the  $\log(g)$  derivation is slightly more accurate. For the faintest stars, with  $G_{RVS} > 13 - 14$ , a  $T_{eff}$  estimate from the BP/RP spectrophotometry is necessary to allow a good

final RVS-based characterization.

#### 4.1.3 Gaia releases

The Gaia mission is designed to operate for five years, with the possibility of 12 to 18 months extension. The data have no proprietary rights and will be released at planned intervals over the mission lifetime, after a proper validation and with increasing details in the data released. The release of the final catalog is planned for 3 years after the end of the mission, i.e., around 2022 or 2023 (see the Gaia data release page for updates).

The first data release is scheduled for the end of summer 2016, and will contain positions and  $G$ -band photometry for single stars from  $\sim 90\%$  of the sky, and data from the ecliptic pole regions that were scanned more often during commissioning. It will also deliver positions, parallaxes and proper motions for a fraction of the 2.5 million Tycho-2 stars (Høg et al. 2000). These astrometric data will be obtained by combining the positions from the Tycho-2 Catalogue with the first year of Gaia data for a joint Tycho-Gaia astrometric solution (TGAS, Michalik et al. 2015; see also the Gaia webpage). Thanks to the  $\sim 24$  yr time baseline, these data will have sub-mas accuracy. The second data release is currently planned for summer 2017, to deliver radial velocities for non-variable bright stars, two-band (BP/RP) photometry, and full astrometric data where available (90% of the sky, only single stars). Two more data releases are planned around 2018-19. Each release updates the previous ones and should contain significant new additions, including astrophysical parameters and classification, mean radial velocities, orbital solutions for binaries, variable star classification, and solar system results. The final catalog should be consisting of:

- Full astrometric, photometric, and radial-velocity catalogues;
- All available variable-star and non-single-star solutions;
- Source classifications and astrophysical parameters (derived from BP/RP, RVS, and astrometry) for stars, unresolved binaries, galaxies, and quasars;
- An exo-planet list;
- All epoch data for all sources;
- All ground-based observations made for data-processing purposes.

## 4.2 Clusters and Gaia

Accurate parallaxes and proper motions provided by the Gaia mission will bring us into a new era of open cluster and association research. Gaia will measure parallaxes and thus distances of *individual* stars with a precision better than 1% if closer than  $\sim 1$  kpc and better than 10% otherwise. Unprecedented accuracies are expected for proper motions, yielding a precision on *individual* tangential velocities of the order of 10 m/s and below for very nearby clusters ( $< 100$  pc), and better

than 1 km/s for FGK stars in clusters up to 1 kpc and up to larger distances for bright O/B stars. Gaia will also provide good photometric information for all objects observed astrometrically, as well as radial velocities and spectroscopic characterization for the 15% brighter.

Gaia will thus deliver a dataset, for both known and possibly newly discovered clusters and associations, that will have a huge impact on a large variety of topics on young cluster research. A non-comprehensive list is given below.

### **Dynamics of open clusters and associations: formation and evolution**

Cluster origin theories range from highly dynamic models (Bonnell et al. 2003) to quasi equilibrium and/or slow contraction scenarios (Tan et al. 2006). The two scenarios lead to different initial cluster structure and kinematics. For example, shallow or absent velocity gradients are expected if clusters form in a quasi-equilibrium state, while strong gradients should be present if clusters form in sub-virial conditions (e.g., Proszkow et al. 2009). In particular, the properties of ejected stars that will be kinematically recovered by Gaia will be vital for constraining the dynamics of star forming regions. For example their age distribution will provide constraints on the timescale of star formation, distinguishing between slow (Krumholz et al. 2005) and rapid (Ballesteros-Paredes et al. 1999) models of star formation. Their spatial and kinematics properties at birth will be obtained by tracing them back to their natal regions, which will reveal the initial structure and density of star forming regions, as well as any possible cluster rotation and kinematic substructures.

Gaia will also provide an opportunity to address questions such as whether OB associations are expanding star clusters or whether they form with low densities (Wright et al. 2014), and whether massive stars can form in isolated or low-density environments, or whether they have been dynamically ejected from dense regions (Bressert et al. 2012). It should in particular be possible to resolve the origins of OB associations by tracing back the motions of their members to see if they represent an expanded star cluster. For simple systems this may be possible with early Gaia data, though more complex arrangements of multiple expanding star clusters will require parallaxes and more precise proper motions from later data releases.

Moreover, a common model of star formation suggests that most stars are born in clusters, but that the majority of these clusters become gravitationally unbound when feedback disperses the gas left over from star formation and get disrupted. This theory of cluster disruption, often referred to as residual gas expulsion, predicts that a large fraction of young and non-embedded star clusters should be supervirial and in the process of expanding. Kinematic Gaia data will be fundamental to address this issue as it will provide a measurement of the dynamical state of a cluster or association, either using proper motions and/or radial velocities (after correction for the broadening of the velocity dispersion due to binaries). Such studies will provide an indication of whether the regions are in virial equilibrium or in the process of collapsing or expanding, and thus constrain any possible effect of residual gas removal.

Also, depending on several factors such as initial conditions themselves, SF efficiency, tidal interaction with the Galaxy, clusters can undergo infant mortality on very short timescales ( $< 10 - 30$  Myr; e.g., Fall 2006) or experience longer term dissolution (De Grijs & Parmentier 2007). In order to understand cluster evolution and to put constraints on those parameters which essentially determine whether the cluster will disrupt into the field or not, realistic simulations are needed. While progress has been made during the past years in the development of these (e.g., Tasker et al. 2008; Capuzzo-Dolcetta 2010), the vital missing element is a large body of observations to be compared with these models, which will be provided by Gaia. N-body numerical simulations of cluster dynamical evolution make indeed many predictions that will be tested using kinematics from Gaia, including how the velocity dispersions of stars vary as a function of stellar mass and environment, the evolution of mass segregation, the expansion and evaporation of star clusters, and their distortion due to the galactic tidal field that can be studied using proper motions.

**Stellar structure and evolution** Gaia will determine accurate distances of a few hundred star clusters in our galaxy for which complete and accurate lists of members will be available. This will finally make fully accessible the unique potential of open clusters to empirically resolve the Hertzsprung-Russell diagram (HRD) and to put tight constraints on the so far still quite limited calibrations of stellar evolutionary models for Pop. I stars, from the pre-main sequence (PMS) phase up to the latest evolutionary stages. Indeed, input physics (opacities, EOS, treatment of convection, mixing, rotation, magnetic fields, He abundances) that significantly influences the stellar luminosity, lifetime and burning-phase duration, still need to be calibrated (e.g., Naylor 2009; Soderblom 2010). Reliable stellar masses and ages can be determined only once the models are appropriately adjusted to represent the data for a wide range of open clusters of different ages and compositions. This is vital for all areas of stellar and galactic astrophysics. Individual distances and photometry provided by Gaia for nearby open clusters and for large samples of members, covering a wide range of spectral types and masses, will yield exquisitely precise colour magnitude diagrams (CMDs) which will be translated into a set of observed isochrones. A comparison of these isochrones with those obtained through modelling will enable us to adjust the models and learn more about stellar evolution, stellar structure and stellar atmospheres.

**The population and evolution of the Galactic thin disk** Key questions are how clusters populate the Milky Way thin disk and what they tell us about its formation and evolution. To answer the first question, we need the data for many OCs at a wide range of Galactocentric radii ( $R_{GC}$ ), and with a large range of ages. The unprecedented accuracy of the astrometric Gaia data will allow us to identify stars sharing the same kinematics, yielding the discovery of new clusters and associations up to 5kpc away from the Sun. High resolution spectroscopic data will then be crucial in order to check that the new groups are not just streams but

that their members share the same origin, i.e., have the same radial velocity, the same age, and the same abundance pattern.

The very young clusters trace the areas of star formation, while older clusters trace the dispersion. The survival rate of OCs as a function of age can be used to trace the history of field star populations (e.g., de Grijs 2010). OCs of different ages and  $R_{GC}$  also reveal information on the radial abundance gradient in the thin disk and on its evolution (e.g., Randich et al. 2005; Bragaglia & Tosi 2006). This is a key input to models of formation and evolution of the disk as metallicity may affect the SF efficiency and the shape of the initial mass function, which will be much better constrained with Gaia. Thanks to the very precise proper motion measurements, ejected cluster members will be recovered by tracing them back to their natal regions, providing a complete census down to the substellar regime for the closest and/or less extincted ones. This will allow us to be much less sensitive to incompleteness and to the cluster dynamical evolution when inferring its luminosity function and IMF.

The abundance gradient at different ages is also essential for assessing the radial streaming of gas (e.g., Schönrich & Binney 2009), the co-rotation resonance, the influence of the bulge, the nature of infall from the halo, and the recent history of our Galaxy spiral pattern as well as the role of possible mergers (e.g., Magrini et al. 2009). Current estimates of the gradient suffer from low number statistics, lack of homogeneity, of samples at key positions/ages, and of orbit determinations (e.g., Magrini et al. 2010). Key new information that will be provided by Gaia are accurate distances from the Sun, allowing to reduce the uncertainties in Galactocentric radii, and proper motions. Additional high resolution spectroscopy will then be necessary for accurate abundance determination of several elements in order to put constraints on previous generations of polluters and to reconstruct the chemical evolution of the disk.

### 4.3 Complementary studies and future facilities

Despite its extraordinary accuracy in parallaxes, positions and proper motions, one of the main limitation of Gaia is its spectroscopic capability. Not only is the limiting distance for radial velocity measurements smaller than for photometry and astrometry (only stars brighter than  $G = 16$  mag will have a spectroscopic observation), but the expected accuracy (1 km/s at best) is much below that expected for the transverse velocity, especially for the brightest objects ( $G < 12 - 13$ ). Moreover, abundance determinations will be possible only for stars brighter than  $G = 12$ .

The other strong limitation of Gaia is that it observes in the optical. As such, it is blind to faint very red objects and sources in extincted regions. Looking for brown dwarfs in star forming regions will thus remain a challenge and will only be possible in close and not too embedded regions.

Complementary data are thus required to obtain more accurate ( $< 1$  km/s) radial velocities and get proper motions at fainter magnitudes and in extincted regions, as well as to measure abundance patterns. Below is a non-exhaustive



list of existing and future surveys that will greatly complement Gaia data. P.I. observations may however still be required to obtain high resolution spectroscopic data and/or deeper and NIR proper motions for specific regions.

#### 4.3.1 On-ground spectroscopic studies

**RAVE** RAVE (RAAdial Velocity Experiment) is a multi-fiber spectroscopic astronomical survey of stars in the Milky Way using the 1.2-m UK Schmidt Telescope of the Australian Astronomical Observatory (AAO).

From 2003 to 2013 (end of observation campaign), RAVE has covered 20,000 square degrees of the sky, obtaining spectra for about 500,000 stars in the magnitude range  $8 < I < 12$  mag, and with a distance up to  $\sim 3$  kpc from the Sun. The covered spectral region contains the infrared Calcium triplet and is similar to the wavelength range chosen for Gaia’s Radial Velocity Spectrometer. The effective resolution of  $R \sim 7,000$  enables radial velocity measurements with a median precision better than 1.5 km/s, as well as good precision atmospheric parameters (effective temperature and surface gravity) and chemical abundances for the surveyed stars.

The RAVE database is public and can be accessed from the RAVE website (<https://www.rave-survey.org/>).

**GALAH** The GALactic Archeology with HERMES project started in 2014 (see <https://galah-survey.org/home>). Observations are carried out with HERMES, a multi-fibre spectrograph operating on the 3.9 m Anglo-Australian telescope, in four wavelength ranges in the visible covering up to 30 different elements with a resolution  $R \sim 28,000$ . The instrument uses the existing 2dF optical fibre positioner to place the 400 fibres over a two-degree field of view. The survey is limited to stars brighter than  $V = 14$ . Even so, it is providing a very important “all-sky” (below +10 deg declination) complement to Gaia, delivering high quality elemental abundances for almost a million stars. GALAH uses open and globular clusters for calibrating purposes.

**Gaia-ESO Survey (GES)** The public spectroscopic Gaia-ESO survey, is targeting more than 100,000 stars using FLAMES at the VLT, and covers the bulge, thick and thin disks and halo components, as well as a significant sample of 100 open clusters of all ages and masses.

The survey uses the GIRAFFE and UVES spectrographs to measure detailed abundances for at least 12 elements (Na, Mg, Si, Ca, Ti, V, Cr, Mn, Fe, Co, Sr, Zr, Ba) in up to 10,000 field stars with  $V < 15$  mag and for several additional elements (including Li) for more metal-rich cluster stars. The radial velocity precision for this sample is 0.1 to 5 km/s, depending on target, and about 0.2 km/s for open cluster stars (Jackson et al. 2015).

Public Gaia-ESO Survey Science Archive can be found at <http://ges.roe.ac.uk/>.

**APOGEE** The Apache Point Observatory Galactic Evolution Experiment (APOGEE) was one of the programs of SDSS-III. The survey consists of high-resolution ( $R \sim 22,500$ ), high signal-to-noise ( $S/N > 100$ ) near-infrared spectra (wavelength range from 1.51 to 1.70  $\mu\text{m}$ ) of mainly 100,000 red giant stars across the full range of the Galactic bulge, bar, disk, and halo using the 2.5m Sloan telescope. APOGEE North and South (also known as APOGEE-2) is now extending this survey in the southern hemisphere using also the 2.5m du Pont Telescope at Las Campanas Observatory in Chile, and targeting  $\sim 300,000$  stars down to  $H \sim 13$ . The radial velocity precision is around 0.1 km/s and the abundance precision is 0.1 dex for more than 15 elements.

Open clusters have also been targeted with APOGEE and APOGEE-2 yielding the Open Cluster Chemical Abundances and Mapping (OCCAM) survey (Frinchaboy et al. 2013), and the INfrared Survey of Young Nebulous Clusters (IN-SYNC, e.g. Cottaar et al. 2014).

#### 4.3.2 On-ground proper motion surveys

**UKIDSS/GCS** The Galactic Cluster Survey (GCS) was one of the five UKIDSS surveys dedicated to open clusters. The GCS imaged 10 open star clusters and star formation associations, covering a total area of 1400 sq. degs, in  $JHK$  to a depth  $K = 18.7$ . The GCS has been completed in two stages. The first stage was a single pass in  $JHK$  over 1400 sq. deg. while the second stage was an additional pass in  $K$  over the same 1400 sq. deg., for proper motion measurements, with a time baseline of 2 to 7 years and a typical accuracy of 2-6 mas/yr (e.g. Lodiou et al. 2012).

The UKIDSS data can be accessed from the WFCAM Science Archive (WSA, <http://wsa.roe.ac.uk/>).

**Pann-STARRS** Pan-STARRS (Panoramic Survey Telescope & Rapid Response System, <http://pan-starrs.ifa.hawaii.edu/public/>) is a wide-field imaging facility developed at the University of Hawaii's Institute for Astronomy and located at Haleakala. The first telescope (PS1) is a 1.8 meter telescope with a 3.2 degree diameter field of view and is equipped with a 1.4 Gigapixel Camera. The second telescope PS2 should become operational soon.

The PS1  $3\pi$  survey produced a catalog of more than three billion objects north of  $-30$  declination with astrometric precision down to 10 milliarcseconds per observation. This excellent calibration and the multiple observations of each point of the sky over a five year internal baseline (60 epochs for each stars, twelve each in 5 filters) allow proper motions as small as 1-2 mas/yr to be measured. The observational schedule has been designed to optimize parallax measurements for red objects. The final parallax and proper motion catalog will enable searches for and classification of stars in the local solar neighborhood, with proper motion searches extending to 200 parsecs.

All the data of PS1 surveys will become public at the end of the PS1 science mission.

**DANCe** The Dynamical Analysis of Nearby Clusters (DANCe) project (<http://www.project-dance.com>) is an ambitious ground based survey aiming at measuring precise proper motions for millions of faint stars in young nearby clusters, taking advantage of archival wide-field surveys. Using the Pleiades as a test bench, Bouy et al. (2013) have developed a powerful collection of softwares for the processing of large amounts of wide-field images from various instruments to provide astrometric (proper motions) and photometric catalogs. 17,000 archival and new images obtained over 15 years and covering  $80 \text{ deg}^2$  in the Pleiades have been combined to reach a final accuracy between 0.3 and 1 mas/yr for all the stars in the magnitude range  $i = 12 - 23$  (see Figure 9). DANCe is four magnitudes deeper than Gaia, reaching the planetary mass domain and piercing through the dust obscured young clusters inaccessible to Gaia’s optical sensors. The extension of this pilot study is named COSMIC-DANCE and will cover 20 young ( $< 120 \text{ Myr}$ ) and nearby ( $< 410 \text{ pc}$ ) clusters and associations, including Gaia-ESO targets when possible.

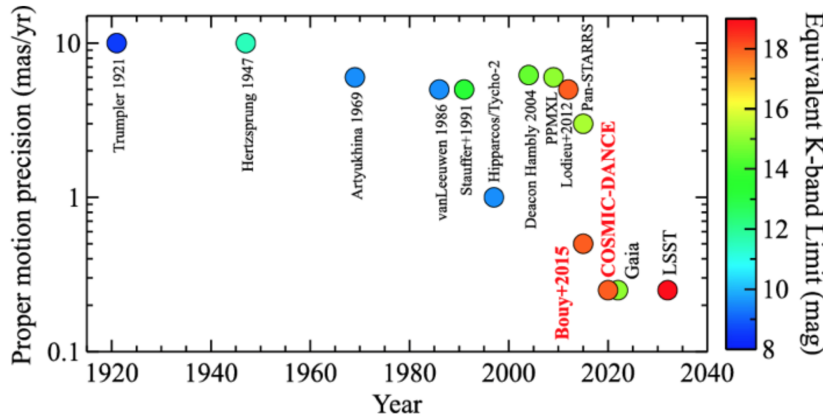


**Fig. 9.** 100 years of proper motion studies in the Pleiades. COSMIC-DANCE can improve the precision and depth by an order of magnitude, and remain unsurpassed until LSST ends in 2032. For optical surveys, the equivalent K-band limit was estimated using typical colours of Pleiades members. Courtesy from H. Bouy.

#### 4.3.3 Future facilities

Several optical/near-infrared high-resolution multi-object spectrographs are currently under development in order to be able to measure precise radial velocities and abundance patterns to follow-up Gaia.

WEAVE (<http://www.ing.iac.es/weave/>) is a new multi-object survey spectrograph for the 4.2m William Herschel Telescope at the Observatorio del Roque de los Muchachos, on La Palma in the Canary Islands. It will allow to take optical spectra of up to 1000 targets over a two-degree field of view in a single exposure. The fibre-fed spectrograph comprises two arms, one optimised for the blue and one

for the red, and offers observations at  $R \sim 5000$  over the full 370-1000nm wavelength range in a single exposure, or a high resolution mode with limited coverage in each arm at  $R \sim 20,000$ . The system integration has now started and the first light at the telescope is expected early 2018.

MOONS at the VLT (<http://www.roe.ac.uk/~ciras/MOONS/VLT-MOONS.html>) should be available one year after (in 2019). The baseline design consists of  $\sim 1000$  fibers deployable over a field of view of  $\sim 500$  square arcmin. The total wavelength coverage is  $0.6\mu\text{m}-1.8\mu\text{m}$  with two resolution modes. In the medium resolution mode ( $R \sim 4000 - 6000$ ) the entire wavelength range is observed simultaneously, while the high resolution mode covers simultaneously three selected spectral regions: one around the CaII triplet (at  $R \sim 9,000$ ) to measure radial velocities, and two regions at  $R \sim 20,000$  (one in the  $J$ -band and one in the  $H$ -band) for detailed measurements of chemical abundances.

4MOST (<https://www.4most.eu/>) is a fibre-fed spectroscopic survey facility on the 4m ESO/VISTA telescope that will be able to simultaneously obtain spectra of  $\sim 2400$  objects distributed over a 4 square degrees field of view. To reach maximum impact, it will operate continuously for an initial five-year Public Survey delivering spectra for  $> 25$  million objects over  $> 15,000$  square degrees at  $R \sim 5000$  and  $\sim 2$  million targets at  $R \sim 20,000$ . 4MOST is currently in its Preliminary Design Phase with an expected start of science operations in 2021.

Finally, the Maunakea Spectroscopic Explorer (MSE, <http://mse.cfht.hawaii.edu/>) is a project to build a 10-meter class telescope replacing the CFHT, and fully devoted to spectroscopy. The single dedicated MSE instrument is a fibre-fed multi-object spectrograph, capable of gathering light from up to 3200 simultaneous objects, each being measured with spectral resolution from  $R \sim 2000$  over the entire 370-1300nm wavelength range to about 20,000 over a restricted range. MSE would be a survey instrument.

Concerning future photometric facilities for proper motions measurements, the Large Synoptic Survey Telescope (LSST, see <http://www.lsst.org/>) is probably the most awaited one. It will produce a 6-band (corresponding to the *ugrizy* filters from 0.3-1.1 micron) wide-field deep astronomical survey of over 20,000 square degrees of the southern sky (south of  $+10$  deg declination) down to  $r \sim 28$  AB mag using an 8.4-meter ground-based telescope. Each patch of sky will be visited about 1000 times in ten years thanks to the very large field of view of the telescope (about 10 sq.deg.). The expected parallax and proper motion accuracy for a ten-year long baseline is 0.6 mas and 0.2 mas/yr at  $r \sim 21$ , and 2.9 mas and 1 mas/yr at  $r \sim 24$ . This is fairly similar to Gaia performance for faint objects, but the real advantage of the LSST is that it will be much deeper (by almost 6 magnitudes) and is more sensitive to distant and red or extincted objects. For example, proper motion of about 200 million F/G main-sequence stars will be detected out to a distance of 100 kpc; complete census of faint populations in nearby star forming regions using color and variability selection will be obtained; deep and highly accurate color-magnitude diagrams for over half of the known globular clusters, including tangential velocities from proper motion measurements, will be created; the Milky Way's halo and the Local Group out to 400 kpc will be mapped. The

LSST is currently being built in Chile and full science operations for the ten-year survey should begin in 2023.

Although not wide field, the JWST (with a launch planned for 2018) and the E-ELT (expected for 2024) are also very much awaited. They will particularly be vital to probe the core of extinguished star forming regions thanks to their unprecedented sensitivity in the infrared. Moreover, the E-ELT will benefit from an exquisite spatial resolution that will provide access to crowded/distant regions for the first time and allow the characterization of very faint/multiple objects. This will allow for example i) to obtain the subsolar census of young massive clusters and more distant environments such as the LMC/SMC in order to test for the IMF universality at high density and/or low metallicity; ii) to measure their internal dynamics and parallaxes from astrometry (precision  $\sim 50\mu\text{as}$ ), and iii) to probe short separation and very low mass ratio binaries in nearby clusters.

Thanks to the above facility developments and the existing surveys, we are now in a really good position to take full advantage of the wealth of Gaia data. This will truly revolutionize our view of the formation and evolution of clusters and associations, of the stars themselves and of the Galactic thin disk as a whole as we will have access for the first time to the 6 phase-space dimensions of the solar neighborhood up to 1kpc (and then 100kpc with LSST), and to accurate photometry and abundances.

## 5 Conclusion

It is clear that the Gaia mission is going to revolutionize our understanding of the stellar cluster formation and evolution as well as our view of the Milky Way. To fully exploit the immense amount of data coming from both Gaia and complementary programmes one needs to be prepared however. The data analysis will require new statistical tools to efficiently study young stars and star clusters in 6-dimensional phase space (three position and three velocity dimensions), as well as folding in a wealth of multi-dimensional data.

Moreover, hybrid hydrodynamic and N-body simulations of star forming regions are needed to link the collapse of molecular clouds with the dynamical evolution of young embedded stellar clusters. We will need many simulations that cover a wide variety of initial and final conditions as well as a number of new statistical diagnostics that will allow us to quantitatively compare observations and simulations. These diagnostics will have to be extensively tested against simulations to make sure that they reliably trace the cluster evolution and that they can be used to resolve the initial conditions.

## References

- Adams, T., Davies, M. B., Jameson, R. F., & Scally, A. 2002, MNRAS, 333, 547
- Alessi, B. S., Moitinho, A., & Dias, W. S. 2003, A&A, 410, 565
- Altmann, M., Edelmann, H., & de Boer, K. S. 2004, A&A, 414, 181

- Andersen, M., Gennaro, M., Brandner, W., et al. 2016, arXiv:1602.05918
- Andreuzzi, G., Bragaglia, A., Tosi, M., & Marconi, G. 2011, MNRAS, 412, 1265
- Ballesteros-Paredes, J., Hartmann, L., & Vázquez-Semadeni, E. 1999, ApJ, 527, 285
- Baraffe, I., Chabrier, G., & Gallardo, J. 2009, ApJL, 702, L27
- Bastian, N., Covey, K. R., & Meyer, M. R. 2010, ARA&A, 48, 339
- Basu, S., Gil, M., & Auddy, S. 2015, MNRAS, 449, 2413
- Bailer-Jones, C. A. L., Andrae, R., Arcay, B., et al. 2013, A&A, 559, A74
- Benjamin, R. A. 2008, Massive Star Formation: Observations Confront Theory, 387, 375
- Bica, E., Dutra, C. M., & Barbuy, B. 2003, A&A, 397, 177
- Binney, J. & Tremaine, S. 1987, Nature, 326, 219
- Bobylev, V. V., Bajkova, A. T., & Lebedeva, S. V. 2007, Astronomy Letters, 33, 720
- Bonatto, C., & Bica, E. 2011, MNRAS, 415, 2827
- Bonatto, C., Kerber, L. O., Bica, E., & Santiago, B. X. 2006, A&A, 446, 121
- Bonnell, I. A., Bate, M. R., & Vine, S. G. 2003, MNRAS, 343, 413
- Bouvier, J., Kendall, T., Meeus, G., et al. 2008, A&A, 481, 661
- Bouy, H., Bertin, E., Moraux, E., et al. 2013, A&A, 554, A101
- Bouy, H., Bertin, E., Sarro, L. M., et al. 2015, A&A, 577, A148
- Bovy, J., Allende Prieto, C., Beers, T. C., et al. 2012, ApJ, 759, 131
- Bragaglia, A., & Tosi, M. 2006, AJ, 131, 1544
- Bressert, E., Bastian, N., Evans, C. J., et al. 2012, A&A, 542, A49
- Briceño, C., Hartmann, L., Hernández, J., et al. 2007, ApJ, 661, 1119
- Brunthaler, A., Reid, M. J., Menten, K. M., et al. 2011, Astronomische Nachrichten, 332, 461
- Buckner, A. S. M., & Froebrich, D. 2014, MNRAS, 444, 290
- Bukowiecki, L., Maciejewski, G., Konorski, P., & Strobel, A. 2011, AcA, 61, 231
- Calamida, A., Sahu, K. C., Casertano, S., et al. 2015, ApJ, 810, 8
- Capuzzo-Dolcetta, R. 2010, Memorie della Societa Astronomica Italiana Supplementi, 14, 210
- Carraro, G., Vázquez, R. A., Costa, E., Perren, G., & Moitinho, A. 2010, apJ, 718, 683
- Carraro, G., Geisler, D., Villanova, S., Frinchaboy, P. M., & Majewski, S. R. 2007, A&A, 476, 217
- Cartwright, A., & Whitworth, A. P. 2012, MNRAS, 423, 1018
- Cartwright, A., & Whitworth, A. P. 2004, MNRAS, 348, 589
- Cescutti, G., Matteucci, F., François, P., & Chiappini, C. 2007, A&A, 462, 943
- Chabrier, G. 2005, The Initial Mass Function 50 Years Later, 327, 41
- Chen, L., Hou, J. L., & Wang, J. J. 2003, AJ, 125, 1397
- Chiappini, C., Matteucci, F., & Romano, D. 2001, ApJ, 554, 1044
- Choi, Y. K., Hachisuka, K., Reid, M. J., et al. 2014, ApJ, 790, 99
- Cottaar, M., Covey, K. R., Foster, J. B., et al. 2015, ApJ, 807, 27
- Cottaar, M., & Hénauld-Brunet, V. 2014, A&A, 562, A20
- Cottaar, M., Covey, K. R., Meyer, M. R., et al. 2014, ApJ, 794, 125
- Cottaar, M., Meyer, M. R., & Parker, R. J. 2012, A&A, 547, A35

- Czekaj, M. A., Robin, A. C., Figueras, F., Luri, X., & Haywood, M. 2014, *A&A*, 564, A102
- Da Rio, N., Gouliermis, D. A., Rochau, B., et al. 2012, *MNRAS*, 422, 3356
- de Boer, K. S., Aguilar Sanchez, Y., Altmann, M., et al. 1997, *A&A*, 327, 577
- de Grijs, R., & Parmentier, G. 2007, *ChJAA*, 7, 155
- de Grijs, R. 2010, *Philosophical Transactions of the Royal Society of London Series A*, 368, 693
- De Marchi, G., Paresce, F., & Portegies Zwart, S. 2005, *The Initial Mass Function 50 Years Later*, 327, 77
- De Marchi, G., Paresce, F., & Pulone, L. 2007, *ApJL*, 656, L65
- De Marchi, G., Paresce, F., & Portegies Zwart, S. 2010, *ApJ*, 718, 105
- De Silva, G. M., Sneden, C., Paulson, D. B., et al. 2006, *AJ*, 131, 455
- de Wit, W. J., Bouvier, J., Palla, F., et al. 2006, *A&A*, 448, 189
- de Zeeuw, P. T., Hoogerwerf, R., de Bruijne, J. H. J., Brown, A. G. A., & Blaauw, A. 1999, *AJ*, 117, 354
- Dias, W. S., Monteiro, H., Caetano, T. C., et al. 2014, *A&A*, 564, A79
- Dias, W. S., Monteiro, H., Caetano, T. C., & Oliveira, A. F. 2012, *A&A*, 539, A125
- Dias, W. S., & Lépine, J. R. D. 2005, *ApJ*, 629, 825
- Dias, W. S., Alessi, B. S., Moitinho, A., & Lépine, J. R. D. 2002, *A&A*, 389, 871
- Dib, S. 2014, *MNRAS*, 444, 1957
- Duchêne, G., & Kraus, A. 2013, *ARA&A*, 51, 269
- Dutra, C. M., Bica, E., Soares, J., & Barbuy, B. 2003, *A&A*, 400, 533
- Fall, S. M. 2006, *ApJ*, 652, 1129
- Famaey, B., Siebert, A., & Jorissen, A. 2008, *A&A*, 483, 453
- Friel, E. D. 2013, *Planets, Stars and Stellar Systems. Volume 5: Galactic Structure and Stellar Populations*, 5, 347
- Friel, E. D., Jacobson, H. R., & Pilachowski, C. A. 2010, *AJ*, 139, 1942
- Friel, E. D., Janes, K. A., Tavaréz, M., et al. 2002, *AJ*, 124, 2693
- Friel, E. D. 1995, *ARA&A*, 33, 381
- Frinchaboy, P. M., Thompson, B., Jackson, K. M., et al. 2013, *ApJL*, 777, L1
- Froebrich, D., Schmeja, S., Samuel, D., & Lucas, P. W. 2010, *MNRAS*, 409, 1281
- Froebrich, D., Scholz, A., & Raftery, C. L. 2007, *MNRAS*, 374, 399
- Fűrész, G., Hartmann, L. W., Szentgyorgyi, A. H., et al. 2006, *ApJ*, 648, 1090
- Galli, P. A. B., Teixeira, R., Ducourant, C., Bertout, C., & Benevides-Soares, P. 2012, *A&A*, 538, A23
- Gennaro, M., Brandner, W., Stolte, A., & Henning, T. 2011, *MNRAS*, 412, 2469
- Gieles, M., & Portegies Zwart, S. F. 2011, *MNRAS*, 410, L6
- Glushkova, E. V., Kopusov, S. E., Zolotukhin, I. Y., et al. 2010, *Astronomy Letters*, 36, 75
- Goodwin, S. P., & Bastian, N. 2006, *MNRAS*, 373, 752
- Gower, J. C., & Ross, G. J. S. 1969, *Applied Statistics*, 18, 54
- Gutermuth, R. A., Megeath, S. T., Myers, P. C., et al. 2009, *ApJS*, 184, 18
- Gutermuth, R. A., Pipher, J. L., Megeath, S. T., et al. 2011, *ApJ*, 739, 84

- Habibi, M., Stolte, A., Brandner, W., Hußmann, B., & Motohara, K. 2013, *A&A*, 556, A26
- Harayama, Y., Eisenhauer, F., & Martins, F. 2008, *ApJ*, 675, 1319
- Heiter, U., Soubiran, C., Netopil, M., & Paunzen, E. 2014, *A&A*, 561, A93
- Høg, E., Fabricius, C., Makarov, V. V., et al. 2000, *A&A*, 355, L27
- Hußmann, B., Stolte, A., Brandner, W., Gennaro, M., & Liermann, A. 2012, *A&A*, 540, A57
- Jackson, R. J., Jeffries, R. D., Lewis, J., et al. 2015, *A&A*, 580, A75
- Jacobson, H. R., Pilachowski, C. A., & Friel, E. D. 2011, *AJ*, 142, 59
- Jacobson, H. R., Friel, E. D., & Pilachowski, C. A. 2009, *AJ*, 137, 4753
- Janes, K., & Adler, D. 1982, *ApJS*, 49, 425
- Janes, K. A., & Phelps, R. L. 1994, *AJ*, 108, 1773
- Janes, K. A., Tilley, C., & Lynga, G. 1988, *AJ*, 95, 771
- Janes, K. A. 1979, *ApJS*, 39, 135
- Jeffries, R. D. 2012, *EAS Publications Series*, 57, 45
- Jeffries, R. D., Maxted, P. F. L., Oliveira, J. M., & Naylor, T. 2006, *MNRAS*, 371, L6
- Jeffries, R. D., Jackson, R. J., Cottaar, M., et al. 2014, *A&A*, 563, A94
- Jordi, C., Gebran, M., Carrasco, J. M., et al. 2010, *A&A*, 523, A48
- Jordi, C., Gebran, M., Carrasco, J. M., et al. 2010, *A&A*, 523, A48
- Kaempf, T. A., de Boer, K. S., & Altmann, M. 2005, *A&A*, 432, 879
- Kharchenko, N. V., Piskunov, A. E., Schilbach, E., Röser, S., & Scholz, R.-D. 2013, *A&A*, 558, A53
- Kharchenko, N. V., Piskunov, A. E., Röser, S., et al. 2009, *A&A*, 504, 681
- Kharchenko, N. V., Piskunov, A. E., Röser, S., Schilbach, E., & Scholz, R.-D. 2005, *A&A*, 440, 403
- Kiminki, D. C., Kobulnicky, H. A., Kinemuchi, K., et al. 2007, *ApJ*, 664, 1102
- Kiminki, D. C., McSwain, M. V., & Kobulnicky, H. A. 2008, *ApJ*, 679, 1478
- King, I. 1962, *AJ*, 67, 471
- Kroupa, P., Weidner, C., Pflamm-Altenburg, J., et al. 2013, *Planets, Stars and Stellar Systems. Volume 5: Galactic Structure and Stellar Populations*, 5, 115
- Kroupa, P. 2002, *MNRAS*, 330, 707
- Kroupa, P. 2001, *MNRAS*, 322, 231
- Krumholz, M. R., McKee, C. F., & Klein, R. I. 2005, *Nature*, 438, 332
- Lada, C. J., & Lada, E. A. 2003, *ARA&A*, 41, 57
- Lamers, H. J. G. L. M., & Gieles, M. 2006, *A&A*, 455, L17
- Lépine, J. R. D., Cruz, P., Scarano, S., Jr., et al. 2011, *MNRAS*, 417, 698
- Lépine, J. R. D., Dias, W. S., & Mishurov, Y. 2008, *MNRAS*, 386, 2081
- Levine, E. S., Blitz, L., & Heiles, C. 2006, *ApJ*, 643, 881
- Lim, B., Chun, M.-Y., Sung, H., et al. 2013, *AJ*, 145, 46
- Lodieu, N., Deacon, N. R., & Hambly, N. C. 2012, *MNRAS*, 422, 1495
- Lodieu et al. 2013, *MNRAS*, 431, 3222
- Luhman et al. 2003
- Lu, J. R., Do, T., Ghez, A. M., et al. 2013, *ApJ*, 764, 155



- Lynga, G. 1982, *A&A*, 109, 213
- Magrini, L., Randich, S., Romano, D., et al. 2014, *A&A*, 563, A44
- Magrini, L., Randich, S., Zoccali, M., et al. 2010, *A&A*, 523, A11
- Magrini, L., Sestito, P., Randich, S., & Galli, D. 2009, *A&A*, 494, 95
- Majewski, S. R. 1993, *ARA&A*, 31, 575
- Malo, L., Doyon, R., Lafrenière, D., et al. 2013, *ApJ*, 762, 88
- Marks, M., & Kroupa, P. 2012, *A&A*, 543, A8
- Maschberger, T. 2013, *MNRAS*, 429, 1725
- Maxted, P. F. L., Jeffries, R. D., Oliveira, J. M., Naylor, T., & Jackson, R. J. 2008, *MNRAS*, 385, 2210
- Melis, C., Reid, M. J., Mioduszewski, A. J., Stauffer, J. R., & Bower, G. C. 2014, *Science*, 345, 1029
- Mermilliod, J.-C. 1992, European Southern Observatory Conference and Workshop Proceedings, 43, 373
- Michalik, D., Lindegren, L., & Hobbs, D. 2015, *A&A*, 574, A115
- Miller, G. E., & Scalo, J. M. 1979, *ApJS*, 41, 513
- Minchev, I., Chiappini, C., & Martig, M. 2014, *A&A*, 572, A92
- Minchev, I., Chiappini, C., & Martig, M. 2013, *A&A*, 558, A9
- Mohanty, S., Stassun, K. G., & Mathieu, R. D. 2009, *ApJ*, 697, 713
- Moitinho, A., Carraro, G., Baume, G., & Vázquez, R. A. 2006, *A&A*, 445, 493
- Moitinho, A. 2001, *A&A*, 370, 436
- Monteiro, H., Dias, W. S., & Caetano, T. C. 2010, *A&A*, 516, A2
- Moraux, E., Bouvier, J., Stauffer, J. R., & Cuillandre, J.-C. 2003, *A&A*, 400, 891
- Moraux, E., Bouvier, J., Stauffer, J. R., Barrado y Navascués, D., & Cuillandre, J.-C. 2007, *A&A*, 471, 499
- Naylor, T., & Jeffries, R. D. 2006, *MNRAS*, 373, 1251
- Naylor, T. 2009, *MNRAS*, 399, 432
- Netopil, M., Pauszen, E., Heiter, U., & Soubiran, C. 2016, *A&A*, 585, A150
- Offner, S. S. R., Clark, P. C., Hennebelle, P., et al. 2014, *Protostars and Planets VI*, 53
- Pancino, E., Carrera, R., Rossetti, E., & Gallart, C. 2010, *A&A*, 511, A56
- Pang, X., Grebel, E. K., Allison, R. J., et al. 2013, *ApJ*, 764, 73
- Parker, R. J., Wright, N. J., Goodwin, S. P., & Meyer, M. R. 2014, *MNRAS*, 438, 620
- Peña Ramírez et al. 2012, *ApJ*, 754, 30
- Perryman, M. A. C., de Boer, K. S., Gilmore, G., et al. 2001, *A&A*, 369, 339
- Piskunov, A. E., Kharchenko, N. V., Schilbach, E., et al. 2008, *A&A*, 487, 557
- Piskunov, A. E., Kharchenko, N. V., Röser, S., Schilbach, E., & Scholz, R.-D. 2006, *A&A*, 445, 545
- Platais, I., Kozhurina-Platais, V., & van Leeuwen, F. 1998, *AJ*, 116, 2423
- Proszkow, E.-M., Adams, F. C., Hartmann, L. W., & Tobin, J. J. 2009, *ApJ*, 697, 1020
- Randich, S., Bragaglia, A., Pastori, L., et al. 2005, *The Messenger*, 121, 18
- Recio-Blanco, A., de Laverny, P., Allende Prieto, C., et al. 2016, *A&A*, 585, A93
- Reid, M. J., Menten, K. M., Brunthaler, A., et al. 2014, *ApJ*, 783, 130
- Rizzuto, A. C., Ireland, M. J., & Robertson, J. G. 2011, *MNRAS*, 416, 3108

- Rochau, B., Brandner, W., Stolte, A., et al. 2011, MNRAS, 418, 949
- Roeser, S., Demleitner, M., & Schilbach, E. 2010, AJ, 139, 2440
- Roškar, R., Debattista, V. P., Quinn, T. R., Stinson, G. S., & Wadsley, J. 2008, ApJ, 684, L79
- Sacco, G. G., Franciosini, E., Randich, S., & Pallavicini, R. 2008, A&A, 488, 167
- Salpeter, E. E. 1955, ApJ, 121, 161
- Sanders, W. L. 1971, A&A, 14, 226
- Sarro, L. M., Bouy, H., Berihuete, A., et al. 2014, A&A, 563, A45
- Schmeja, S., Kharchenko, N. V., Piskunov, A. E., et al. 2014, A&A, 568, A51
- Scholz, A., Geers, V., Clark, P., Jayawardhana, R., & Muzic, K. 2013, ApJ, 775, 138
- Schönrich, R., Binney, J., & Dehnen, W. 2010, MNRAS, 403, 1829
- Schönrich, R., & Binney, J. 2009, MNRAS, 399, 1145
- Sestito, P., Bragaglia, A., Randich, S., et al. 2008, A&A, 488, 943
- Sestito, P., Bragaglia, A., Randich, S., et al. 2006, A&A, 458, 121
- Soderblom, D. R. 2010, ARA&A, 48, 581
- Stassun, K. G., Scholz, A., Dupuy, T. J., & Kratter, K. M. 2014, ApJ, 796, 119
- Stauffer, J. R., Schultz, G., & Kirkpatrick, J. D. 1998, ApJ, 499, L199
- Stolte, A., Brandner, W., Brandl, B., & Zinnecker, H. 2006, AJ, 132, 253
- Tadross, A. L. 2011, Journal of Korean Astronomical Society, 44, 1
- Tan, J. C., Krumholz, M. R., & McKee, C. F. 2006, ApJ, 641, L121
- Tasker, E. J., Brunino, R., Mitchell, N. L., et al. 2008, MNRAS, 390, 1267
- Twarog, B. A., Ashman, K. M., & Anthony-Twarog, B. J. 1997, AJ, 114, 2556
- Van Leeuwen, F. 2009, A&A, 97, 209
- Vázquez, R. A., May, J., Carraro, G., et al. 2008, ApJ, 672, 930-939
- Wright, N. J., Parker, R. J., Goodwin, S. P., & Drake, J. J. 2014, MNRAS, 438, 639
- Xu, Y., Li, J. J., Reid, M. J., et al. 2013, ApJ, 769, 15
- Yong, D., Carney, B. W., & Friel, E. D. 2012, AJ, 144, 95
- Yong, D., Carney, B. W., & Teixeira de Almeida, M. L. 2005, AJ, 130, 597
- Zacharias, N., Finch, C. T., Girard, T. M., et al. 2013, AJ, 145, 44
- Zhang, B., Reid, M. J., Menten, K. M., et al. 2013, ApJ, 775, 79